DESIGN AND OPTIMIZATION OF MEMS ACCELEROMETER SENSOR FOR LOWER LIMB EXOSKELETON APPLICATION

MUHAMMAD FAREQ BIN IBRAHIM

RESEARCH REPORT SUBMITTED IN PARTIAL FULFILMENT OF THE REQUIREMENT FOR THE DEGREE OF MASTER OF ENGINEERING (INDUSTRIAL ELECTRONICS AND CONTROL)

FACULTY OF ENGINEERING

UNIVERSITY OF MALAYA

2018

UNIVERSITI MALAYA

ORIGINAL LITERARY WORK DECLARATION

Name of Candidate: **MUHAMMAD FAREQ BIN IBRAHIM**

Registration/Matrix No.: **KQC160001**

Name of Degree: **Master of Engineering**

Title of Project Paper/Research Report/Dissertation/Thesis ("this Work"): **DESIGN AND OPTIMIZATION OF MEMS ACCELEROMETER SENSOR FOR LOWER LIMB EXOSKELETON APPLICATION**

I do solemnly and sincerely declare that:

(1) I am the sole author/writer of this Work;

(2) This work is original;

(3) Any use of any work in which copyright exists was done by way of fair dealing and for permitted purposes and any excerpt or extract from, or reference to or reproduction of any copyright work has been disclosed expressly and sufficiently and the title of the Work and its authorship have been acknowledged in this Work;

(4) I do not have any actual knowledge nor ought I reasonably to know that the making of this work constitutes an infringement of any copyright work;

(5) I hereby assign all and every rights in the copyright to this Work to the University of Malaya ("UM"), who henceforth shall be owner of the copyright in this Work and that any reproduction or use in any form or by any means whatsoever is prohibited without the written consent of UM having been first had and obtained;

(6) I am fully aware that if in the course of making this Work I have infringed any copyright whether intentionally or otherwise, I may be subject to legal action or any other action as may be determined by UM.

Candidate's Signature Date

Muhammad Fareq Bin Ibrahim

Subscribed and solemnly declared before,

Witness's Signature Date

Name: Designation:

ABSTRACT

Currently a lot of studies have added their focuses into several backgrounds that are known as multi-discipline studies. One of the study is on lower limb exoskeleton which are the combination of electrical, mechanical and biomedical field. Lower limb exoskeleton study evolve on potential of helping disable people to walk again. Lower limb exoskeleton consists of multi components and one of it is the MEMS accelerometer. MEMS accelerometer are used to give an accurate angle at the joint of lower limb exoskeleton because the exoskeleton must be designed to be as similar as possible with the real human's leg. For this reason, an existing study on design of dual-axis MEMS accelerometer have been selected and simulated by using COMSOL Multiphysics. This design will be studied to obtain the optimal results on maximum stress and displacement sensitivity on X-axis and Y-axis. Three parameters have been modified into ±5%, ±10%, ±15%, ±20%, and ±25% to see their effect which are the lengths and widths of the beam and thickness of device. Taguchi method has been used for the optimization to get the optimal results. From the simulation results and analysis, this study was able to get 26.6419% and 60% of improvement of maximum stress and displacement sensitivity on X-axis and 31.8163% and 61.1556% of improvement of maximum stress and displacement sensitivity on Y-axis.

ABSTRAK

Kini, banyak kajian pembelajaran telah menambah fokus mereka kepada beberapa latar belakang yang turut dikenali sebagai pembelajaran bermulti-disiplin. Salah satu kajian adalah terhadap kerangka bahagian lebih rendah angota badan yang menggabungkan bidang elektrik, mekanikal dan biomedik. Kerangka bahagian lebih rendah angota badan ini berguna untuk membantu orang kurang upaya untuk berjalan kembali. Di dalamnya, terdapat multi componen dan *MEMS accelerometer* adalah salah satu daripadanya. *MEMS accelerometer* digunakan untuk memberi sudut secara tepat di bahagian pertemuan kerangka bahagian lebih rendah angota badan kerana kerangka ini perlu direka sehampir mungkin menyamai kaki manusia sebenar. Untuk itu, satu kajian sedia ada terhadap duo-paksi *MEMS accelerometer* telah dipilih dan disimulasi menggunakan *COMSOL Multiphysics*. Rekaan ini kemudian akan diteruskan kajian bagi mendapatkan nilai tekanan maksimum dan kepekaan anjakan ke atas paksi-X dan paksi-Y secara optimum. Tiga parameter iaitu panjang, lebar dan ketebalan peranti telah diubah sebanyak ±5%, ±10%, ±15%, ±20%, dan ±25% bagi melihat kesannya terhadap kedua-dua hasil yang dikehendaki. Bagi tujuan pengoptimuman, kaedah Taguchi telah digunakan bagi mendapatkan hasil paling optimum. Hasil daripada simulasi dan analisis, kajian ini berjaya memperoleh 26.6419% dan 60% penambahbaikan bagi tekanan maksimum dan kepekaan anjakan terhadap paksi-X dan 31.8163% dan 61.1556% penambahbaikan bagi tekanan maksimum dan kepekaan anjakan terhadap paksi-Y.

ACKNOWLEDGEMENT

Alhamdulillah and all praise to Allah s.w.t. that give me chance in completing my project of "**Design and Optimization of MEMS Accelerometer Sensor for Lower Limb Exoskeleton Application**" with such a very shortest time. I would like to express my deepest gratitude to my supervisor, Assoc. Prof. Ir. Dr. Norhayati Soin for giving me the opportunity to conduct my final project under her supervision. The supervision and support that she gave truly help the progression and smoothness of my research project.

Thanks also to my friends Qamar and Suffian, as my roommate at Universiti Malaya (UM) and car-pool together from Melaka to attend the classes. Not forget, all students under same research group Mazita, Aida, Annuar and Norliana for their support on doing simulation and fundamental studies.

To beloved wife, Fadatu Salwa and son, Zuhayr Fayyadh, thank you for your understanding and give me such a space alone in concentrating doing this project. Not to forget my father, mother and siblings as giving me their blessing and motivation in completing this project.

Next, I would like to thank my sponsor and employer, Universiti Teknikal Malaysia Melaka (UTeM) for giving me chance to further my studies with full scholarship. To all my colleagues at UTeM and all my classmate at UM, thank you for helping me with the simulation and giving inputs on how to solve the problem to complete this project. Last but not least, my proof read checker, Syahrul Hisham that helps checked the thesis.

TABLE OF CONTENTS

List of Figures

List of Tables

List of Symbols and Abbreviations

MEMS	Microelectromechanical Systems
FEA	Finite Element Analysis
DOF	Degree of Freedom
CCP	Coupled Cooperative Primitives
KF	Kalman Filter
IC	Integrated Circuit
S/N	Signal-to-Noise
NIB	Nominal is Best
STB	Smaller the Best
LTB	Larger the Best
C	Capacitance
ε	Electric Constant
d	Distance
A	Area
V	Voltage
K_s	Spring constant
m	Mass
D	Damping coefficient

a	Acceleration
ω	Resonant frequency
Q	Quality factor
F	Force
t	Time
ρ	Density
E	Young's modulus
v	Poisson's ratio

CHAPTER 1 : INTRODUCTION

1.1 Overview

Nowadays, Microelectromechanical Systems also known as MEMS have been studies by numerous researchers. One of the MEMS devices, MEMS accelerometer have been studies and it was focus on optimizing of the device stress and displacement sensitivity characteristics. The term "*micro*" in MEMS already give an idea that it were designed as small as possible (in micro size) compared to the other conventional design. Although with the smaller size and lesser weight for MEMS accelerometer, the device still able to functions with higher efficiency and at the other hand, it also contributed to the lower manufacturing costs.

A lot of our everyday life item was design with MEMS accelerometer inside it ranging from telecommunication, car airbag deployment systems and biomedical such as exoskeleton for lower limb as well as upper limb. By detecting the direction of acceleration of upper or lower limb, accelerometers are one of the sensors to use. This sensor able to measure and maintain the orientation, based on the principles of the conservation of momentum and rotation. The changes of these angles are depending on the changes to the types of sensor that will be used in this project which is the capacitance.

1.2 Background Studies

For the last two decades, microelectromechanical sensors (MEMS) have been applied to biomechanics applications which are very helpful for human being. MEMS are used because it have many advantages such as low cost and provide higher efficiencies. Despite it have many advantages, the application of MEMS in biomechanics still experience bias, scale factors and other random errors (Olivares,

Olivares, Gorriz, & Ramirez, 2009; Sabatini, 2011). According to (Stefan Lambrecht, 2016), these errors are due to misalignment of axes in manufacturing of the sensor or during assembly of inertial measurement units (IMU).

Figure 1.1 Upper and lower limb exoskeleton for rehabilitation robotics (Rocon et al., 2007)

Since these exoskeletons required an accurate and precise angle, as mention earlier in this chapter, MEMS accelerometer was used due to it small micro size and the accuracy of the device. The sensor will be connected to microprocessor to obtain data of movement and at same time, it will able to be controlled manually. Figure 1.2 shows an example of MEMS accelerometer that can be used for this application. The specification of the sensor will be discussed more on chapter 2 of this report.

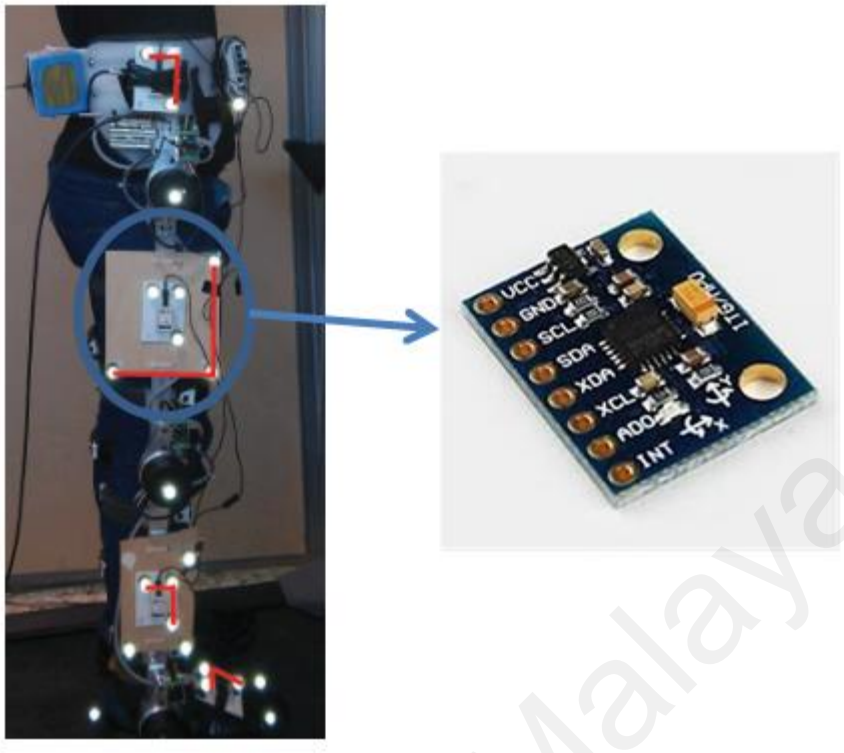

Figure 1.2 MEMS accelerometer at lower limb exoskeleton (Souza, 2015; Stefan Lambrecht, 2016)

1.3 Structural of Lower Limb Exoskeleton

A robotic lower limb exoskeleton has been developed to enable functional compensation of people suffering muscles weakness around the knee and ankle joint (Moreno, Freriks, Porsteinsson, Sánchez, & Pons, 2004). The lower limb exoskeleton follows the kinematic structures of the leg and spans the knee as well as the ankle joints. The exoskeleton is equipped with a collection of kinematic and kinetic sensor to enable the ambulatory monitoring of pathological gait and to help evaluate progress of rehabilitation programmes (Rocon et al., 2007).

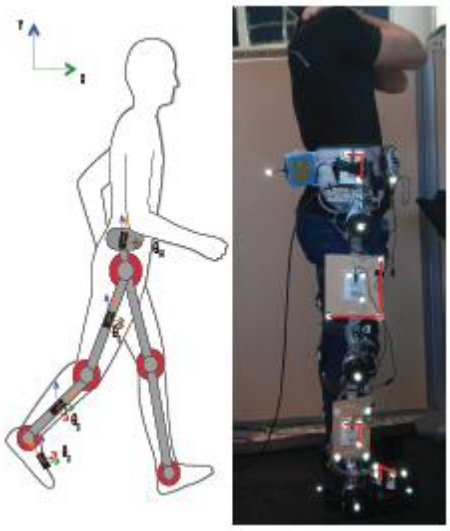

Figure 1.3 The design of lower limb exoskeleton with 6 actuated degrees of freedom and precision accelerometer at every joint (Stefan Lambrecht, 2016)

1.4 Structure Device Design of MEMS Capacitive Accelerometer

There are a lot of reasons why the capacitance was commonly chosen for accelerometer. One of it as mention by (Andrejašic, 2008) was due to the capacitance sensor's interface have a remarkable features in which is very sensitive and at the other hand, it may not easily affected by the temperature.

$$C = \frac{\varepsilon_0 \varepsilon A}{d} \tag{1.1}$$

Referring to equation 1.1, C is equivalent to Capacitance, permittivity was labelled as $\varepsilon_0 \varepsilon$, distance as d and the area as A. The main part of the capacitive accelerometer (also can be called as "housing"), and sometimes it was referred as proof mass or seismic mass will moved the "comb-like" part back and forth. This movement will able the acceleration to be calculated. Due to this movement of the centre area, as a result, the fingers on the accelerometer structure will allowing the current to flow by made up a differential capacitance as mention by (Lee et al., 2005).

$$a = \frac{K_s d}{m V_0} V_x \tag{1.2}$$

Referring to equation 1.2, V_x represents the voltage of the proof mass or the output voltage and x represents the displacement. K_s and m, represents the spring constant and the mass. Based on these parameters, it will obtained the acceleration (Sharma, Macwan, Zhang, Hmurcik, & Xiong, 2007).

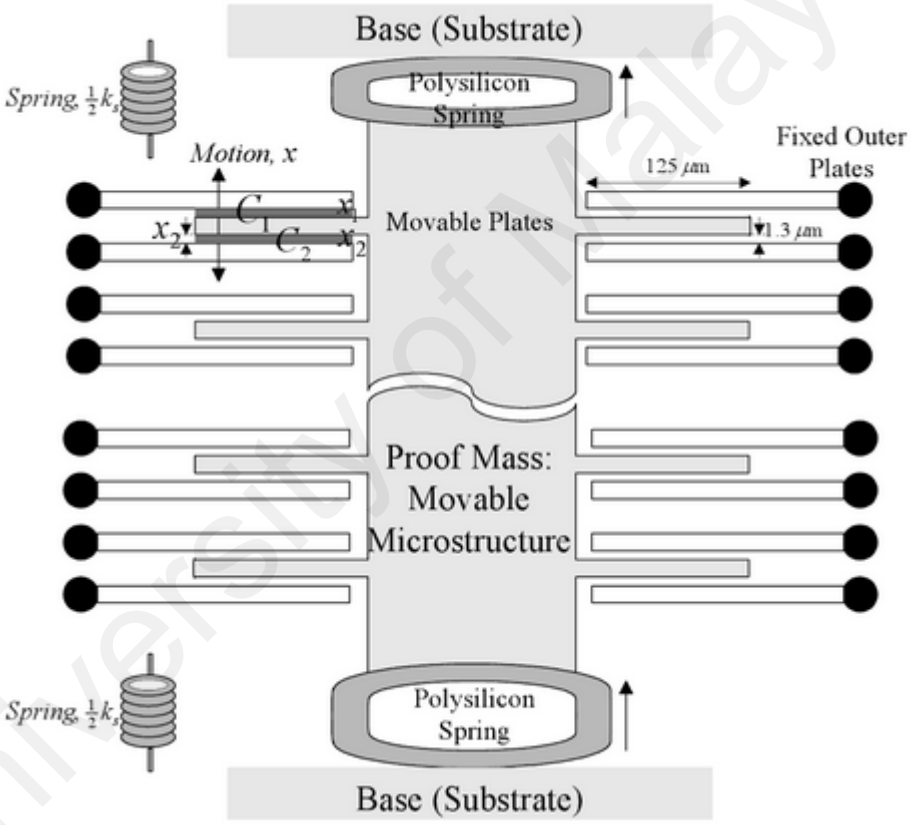

Figure 1.4 Structure of accelerometer where the spring's constant was attached to proof mass at substrate. It able to moved up and down. The capacitor was determined from the moveable and fixed plates (Lyshevski, 2002)

1.5 Finite Element Analysis and Optimization Method

Nowadays, MEMS sensors may capable to be designed and analysed virtually without been manufactured or developed the device physically. This was done by using

the Finite Element Analysis (FEA) in which it will design and analyse virtually MEMS sensor by using the computer simulation. The software will able to predict a detailed outcome of the design before it goes to manufacturing process. By using FEA, a lot of manufacturing cost can be saved since it is not compulsory to manufacture the real device several times to get the desired outcomes. To get more realistic and accurate effects, three dimensional design was commonly used (Widas, 1997). An example of FEA testing is that it able to show how much stress can be applied on the device by using a certain material and for sure, it able to measure the displacement sensitivity of device when applying force on it. FEA really helpful to engineers understand the design of their products and verify the simulation by comparing it with theoretical.

Through FEA, optimization method for the designs can be easily done. For this research project, Taguchi method is used by re-designing the published structure to get higher stress and displacement sensitivity of the device.

1.6 Problem Statements

Limb exoskeleton can be separated into two parts which is lower limb and upper limb exoskeleton. As the name itself, it was designed to help a disable people either lower or upper limb to able use their limb again. For lower limb exoskeleton, people will able to use it for walking again. Research done by (Huang et al., 2016; Rocon et al., 2007; Stefan Lambrecht, 2016) have be done for this lower limb exoskeleton. All of the research was conclude that for lower limb exoskeleton must have a low power frequency, high sensitivity and robust. Inside the exoskeleton consists of microcontroller to control many input sensors such as inertial sensor, gyroscope sensor, accelerometer sensor and magnetometer sensor. Gyroscope sensor is able to make a 6-degree-of-freedom inertial measurement unit. Then, gyroscopes also have accelerometers which is 3-axis accelerometer. Other than that, to form an inertial

measurements unit, it required three sensors: gyroscopes, accelerometer and magnetometer. This inertial measurement is important to give the desired angle for lower limb exoskeleton. In order to design a small size of lower limb exoskeleton, MEMS technology was applied due to its small size.

This study will focus on one of sensor inside lower limb exoskeleton which is MEMS accelerometer. Studies done by (Ce Zheng, 2015; Khairun Nisa, 2014; Shah, Iqbal, & Lee, 2016; Shah, Iqbal, Shah, & Lee, 2016; Sung et al., 2014; Yusof, Soinb, & Noorakma, 2017) have conclude several type of accelerometer sensors with different results. (Sung et al., 2014) have fabricated an accelerometer sensor with high sensitive and robustness to get the expected frequency. Research by (Shah, Iqbal, Shah, et al., 2016) focussed on tri-axis sensor to measure three angular velocity on single drive with Z-shape beam for support folded coupling spring and resulted a different frequency with different sensing spring. Another three-axis MEMS accelerometer have been design by (Shah, Iqbal, & Lee, 2016) which is contained with unique and simple coupling spring to measure the frequency of drive mode, pitch, role and yaw sensing of the accelerometer. Meanwhile, (Khairun Nisa, 2014; Yusof et al., 2017) have studied the effect of several parameters in MEMS accelerometer on the maximum stress and displacement sensitivity. The design of MEMS accelerometer with T-shape beams done by researcher (Ce Zheng, 2015) was simulated by using COMSOL Multiphysics and resulted the maximum stress and displacement sensitivity on X-axis of 4.5594×10^6 Pa and 0.0051578 µm/g while in Y-axis, it give 2.5348×10^6 Pa and 0.0026694 µm/g. This result can be improved and optimal by using the Taguchi method and the objective is to get higher result on maximum stress and displacement sensitivity for both X and Y beams to be applied on lower limb exoskeleton.

1.7 Thesis Objectives

The objective of this project is:

- To optimize a MEMS accelerometer structure to achieve the device maximum stress larger than 4.5594 x 10^6 Pa and 2.5348 x 10^6 Pa for X and Y axis for lower limb exoskeleton application
- To optimize a MEMS accelerometer structure by enhancing the device maximum displacement sensitivity larger than 0.0051578 μm/g and 0.002873 μm/g for X and Y axis for lower limb exoskeleton application

1.8 Scope and Limitation

To increase the displacement sensitivity and maximum stress of MEMS accelerometer, micromachined of the device with certain parameter can be applied. Structure of device is only focuses on simulation design and also analytical analysis.

As for the simulation part, it will cover the Solid Mechanic studies to check the displacement and maximum stress of the device on each X and Y axis of the accelerometer can withstand. After that, the optimization analysis will be done by using Taguchi Method.

Although the objectives of this research is to applied the accelerometer with lower limb exoskeleton, due to limitation of cost and time, this research will only focuses on device itself and shows how the spec of accelerometer are within the need of lower limb exoskeleton.

1.9 Project Methodology

In general, methodology used in this project start with selection of model structure that obtained from literature review. Next, COMSOL Multiphysics simulation

tools will be used to redesign the model before run the simulation in five different variations of selected parameters which is length and width of the X and Y beams and the thickness of device. The data will later analyse and optimize by using Taguchi method. The project methodology will be explained in detail in Chapter 3 of this report.

1.10 Thesis Outline

This report consists of five chapters which is introduction, literature review, project methodology, results and discussion and conclusion. In chapter 1 (introduction), it discussed the overview of background studies with the example of MEMS accelerometer. This chapter also share the selected of finite element analysis, objectives and scope of the project. Meanwhile in chapter 2 (literature review), all the theory of MEMS accelerometer and lower limb exoskeleton will be shared. This all data were presented by understanding and study from various books, journals and articles. Chapter 3 of the report will focused on project methodology where the detail of each step will be further explained. All results obtained in this study will be analysed and shows in chapter 4 of the reports. Last but not least, chapter 5 (conclusion) will conclude the study and works done and all further study that was recommended.

CHAPTER 2 : LITERATURE REVIEW

2.1 Introduction

Micro-Electro-Mechanical Systems, or MEMS, is a technology that in its most general form can be defined as miniaturized mechanical and electro-mechanical elements (i.e., devices and structures) that are made using the techniques of microfabrication. The critical physical dimensions of MEMS devices can vary from well below one micron on the lower end of the dimensional spectrum, all the way to several millimetres.

Over pass 30 years, MEMS accelerometer has been used in various field including automotive, industrial and medical. MEMS accelerometers are commonly used due to its simple structure, simple fabrication process and read out circuit compared to other accelerometer. The problem of this type of sensor is, it cannot simply applied in all application because of different application may require a different parameter.

2.2 Lower Limb Exoskeleton

Lower limb exoskeleton was designed to help disable people to walk again. For this reason, the hip and knee joint must be able to follow the human movement smoothly which means there are motion range need to follow and characteristic of human to be referred. This movement must be within acceptance range of bend in term of angle and speed of bending.

2.2.1 Exoskeleton

Nowadays, there is various type of exoskeleton that designed to help people who have a disability. From these, three major studies were done on upper limb and lower limb. As the name itself, upper limb was design to help patient with disability on their

arm while lower limb to help patient with disability of lower body. As mention earlier in this report, the focus of this research is on lower limb exoskeleton.

2.2.2 Literature Surveys

Several studies have been made on lower limb exoskeleton and Table 2.1 shows summarization of the studies.

In the lower limb exoskeleton, sensors used must give a very precise angle to able a patient to use it as a real leg. In order to give an accurate angle, one of the sensor can be used are accelerometer. Other than that, with the current technology, the exoskeleton must also be designed with a small size of circuit to make it comfortable for the patient and for this reason, MEMS sensors technology was applied on it.

From Table 2.1, there are no specific requirements of accelerometer used. But it is understandable that the sensor must have a low frequency, robust, and have a high sensitivity.

Table 2.1 Summary of other researcher on lower limb exoskeleton

Researcher	Title	Year	Objective	Specification	Output
E. Rocon, J.C. Moreno, A.F. Ruiz, F. Brunetti, J.A. Miranda, J.L. Pons	Application of inertial sensors in rehabilitation robotics	2007	1. Applied an inertial sensors in rehabilitation robotic 2. Identify restriction in the design of the robots in order to use the sensors 3. The design was at upper and lower limb rehabilitation exoskeletons	1. The sensors used was MEMS inertial sensors 2. It required 6-degree of freedom 3. Both acceleration and angular rate consist of 3-axis	1. The cutting frequency of 4 Hz 2. Average walking experiments with speed of 2.6km/h
Rui Huang, Hong Cheng, Hongliang Guo, Xichuan Lin, Qiming Chen, Fushun Sun	Learning cooperative primitives with physical human-robot interaction for a human-powered lower exoskeleton	2016	1. Calculation based on theory on how the movements of lower-limb exoskeleton 2. Do the experiments base on theory obtain	Use the Coupled Cooperative Primitives (CCP) theory to obtain: 1. Dynamic movement primitives 2. Coupled cooperatives primitives	1. Measured the degree of freedom (DOF) 2. The measurements was done at the knee joint
Stefan Lambrecht, Samuel L. Noguera, Magdo Bortole, Adriano A. G. Siqueira, Marco H. Terra, Eduardo Rocon, José L. Pons	Inertial sensor error reduction through calibration and sensor fussion	2016	1. Comparison between cooperative and local Kalman Filter (KF) 2. Estimate absolute segment angle 3. Measured acceleration due to gravity and body motion	1. Experiment done on subject with: 33 years old, 1.75m height and 82kg mass 2. Subject walk at treadmill for 60 seconds period 3. The first and last 10 seconds was ignored 4. 40 seconds data were collected to see the 90 degree expected angle 5. Frequency used for this experiments was 50 Hz	1. From he collected data, it was analysed with Kalman Filter for optimization

2.2.3 Research Study on Lower Limb Exoskeleton

As shown on Table 2.1, three research studies have been reviewed on lower limb exoskeleton to complete this report. First research was done by (Rocon et al., 2007) in which it use an inertial sensors in this exoskeleton. Although it is using an inertial sensors, actually indirectly it can be applied for accelerometer studies as well because for inertial measurement, the sensor used usually a gyroscopes as it is able to make a 6-degree-of-freedom inertial measurement unit. Within the gyroscopes itself also have an accelerometers which is 3-axis accelerometer. Other than that, to form an inertial measurements unit, it required three sensors: gyroscopes, accelerometer and magnetometer.

For this study, (Rocon et al., 2007) have done simulation on upper and lower limb exoskeleton and it will measured the cutting frequency in which give 4 Hz. Figure 2.1 shows how the exoskeleton was designed. Figure 2.2 shows the result in which (Rocon et al., 2007) have the cutting frequency of 4 Hz with average walking experiments of 2.6 km/h.

Figure 2.1 Design of lower limb exoskeleton by (Rocon et al., 2007)

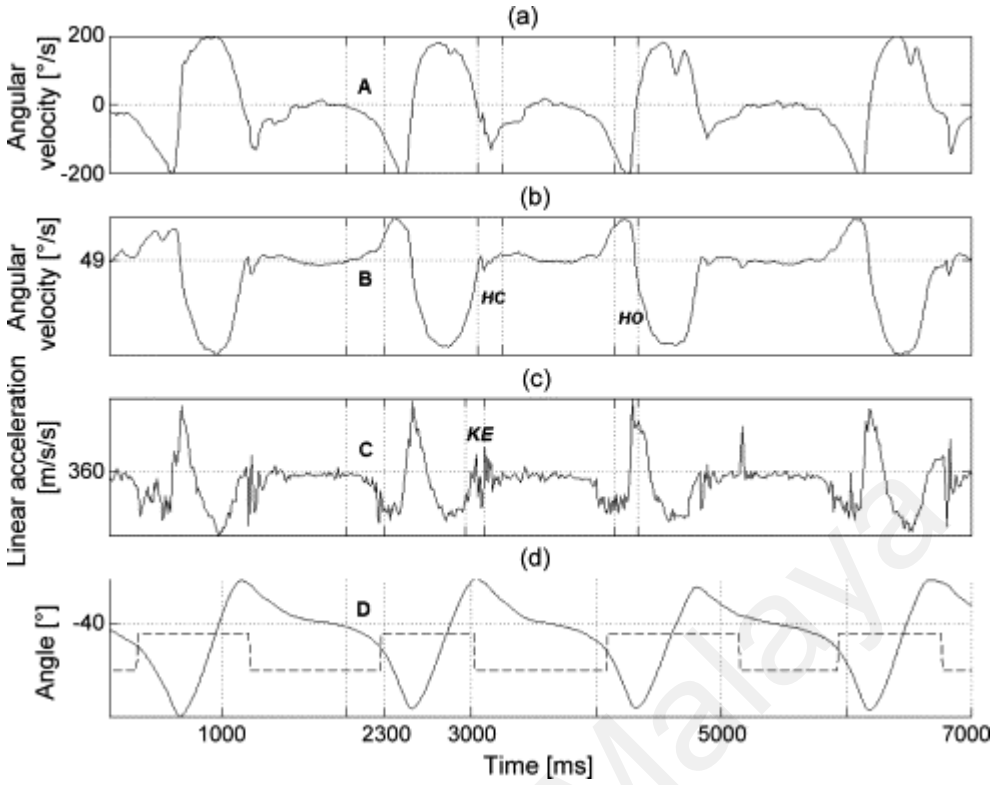

Figure 2.2 (a) orthosis foot plate rotational velocity, (b) lower bar segment rotation velocity; (c) orthosis ankle part linear -Y axis- acceleration and (d) calculated ankle orthosis joint angle - solid line, for a sequence of four gait cycles of a subject wearing the orthosis prototype on level ground. Transition between controlled stance and free swing modes is used as (d) reference signal - dashed line. A, B and C represent periods of feasible and early detection for control. (Rocon et al., 2007)

Second research done by (Huang et al., 2016) was more on measuring the degree of freedom. The design of exoskeleton was designed by using concept as Figure 2.3(a). It was focused on measurement at knee joint and the result was shown in figure 2.3(b).

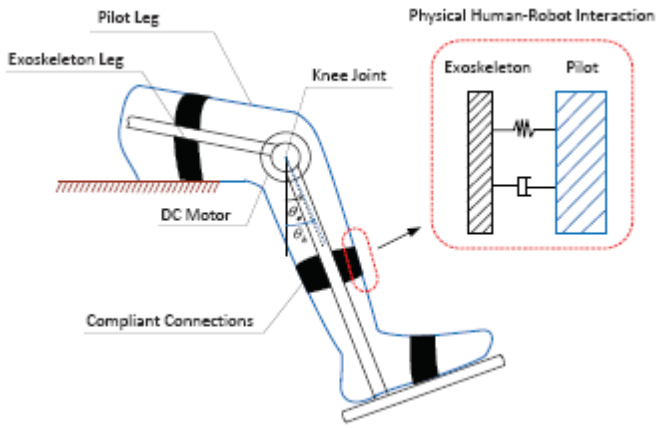

(a)

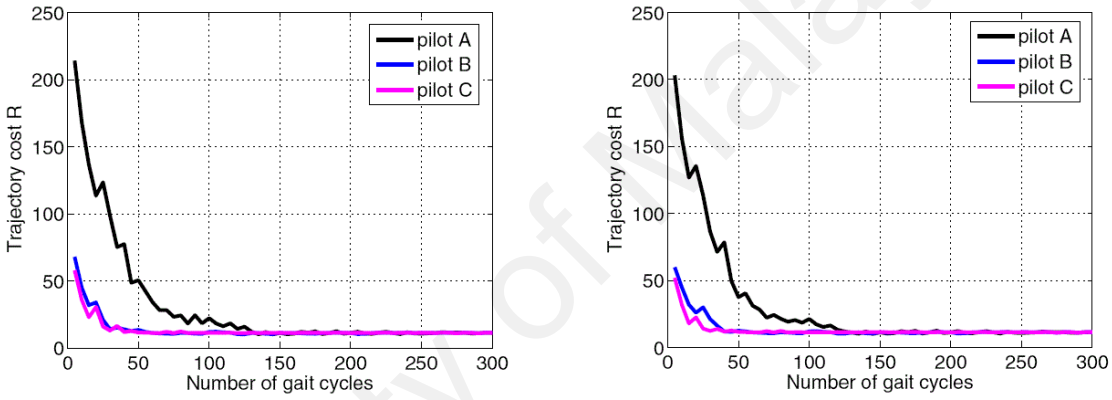

(b)

Figure 2.3 (a) The schematic diagram of lower lib exoskeleton system (b) The degree of freedom (DOF) for knee and hip joint (Huang et al., 2016)

The third research done by (Stefan Lambrecht, 2016), where it is focusing on optimization by using Kalman Filter. Figure 2.4 show the experimental setup where it was applied to a 33 years old man with weight of 82 kg and 1.75 m height. The data collected when subject walk at treadmill for 60 seconds and the first and final 10 seconds data were ignored as it was consider as start and stop error time. In 40 seconds data collected, the measurement done is the accuracy of 40 degree angle and an optimization is done by using Kalman Filter.

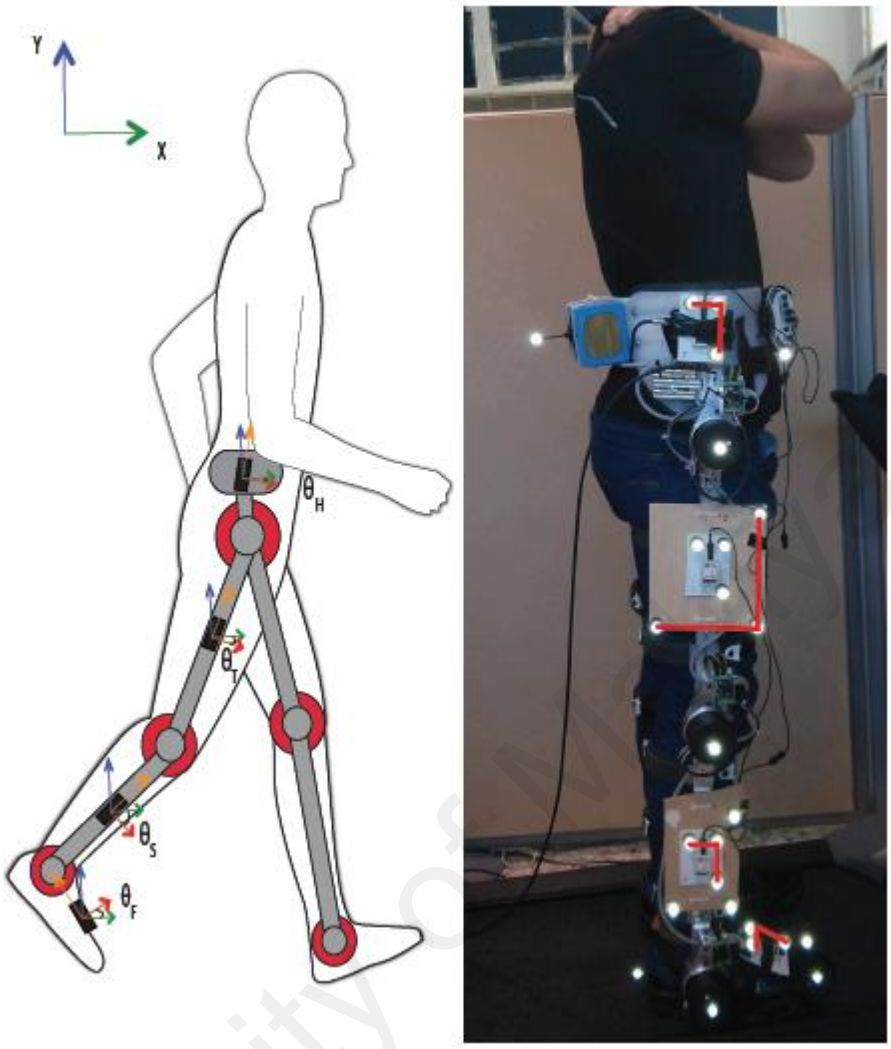

Figure 2.4 Experiment setup with total of 4 inertial sensors attached to the right leg (Stefan Lambrecht, 2016)

Based on three past research, it can be summarized that the lower limb exoskeleton need to have various sensors and one of it is inertial sensor which is combination of gyroscope, accelerometer and magnetometer sensors. All studies were done to check the frequency which is must be low, high sensitivity to give the accuracy of angle and the device must be robust.

2.3 MEMS Accelerometer

2.3.1 Microelectromachanical System (MEMS)

Microelectromechanical System (MEMS) has become an emerging technology that covers from house appliance to automotive and even in medical industry. The remarkable development with MEMS is initiated from the integrated circuit technologies and then evolved into a highly functional systems in miniaturized version. MEMS sensor comes from an input of mechanical signal which is converted using an interface circuit to a corresponding electrical signal that is used to produce the required control function (Gogoi & Mladenovic, 2002).

This incorporation between MEMS sensor with the help of the interface circuit can be done using silicon or packaged it completely. Most MEMS devices are prepared from silicon wafer which are similar to integrated circuit (IC) where MEMS fabrication also shares the same standard process like etching, photolithography oxidation, diffusion and deposition.

2.3.2 Principle of Operation

Interface in capacitance sensor have some great features where it can function equally as an actuator and a sensor. It is highly sensitive but naturally unaffected to current temperature (Tim, 1996).

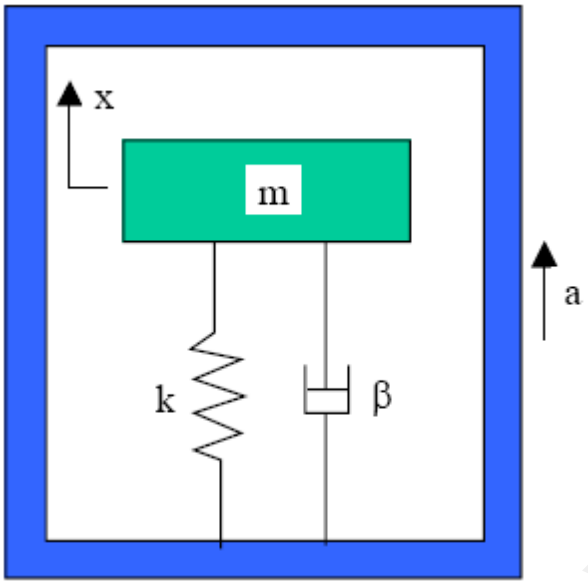

Figure 2.5 Basic accelerometer (Denishev & Petrova, 2007)

To understand the basic operation of accelerometer is by simply using the principle of a mass spring system which is the second order mass-spring-damper system (Vijila, Vijayakumar, & Gupta, 2011).

$$M_s.\frac{d^w x}{dt^2} + D.\frac{dx}{dt} + K_s x = M_s.a_{ext} \tag{2.1}$$

given the spring constant, K_s, the damping coefficient as D, the movable mass as M_s and the external acceleration as a_{ext}.

If the equation (2.1) changes to transfer function of second order using the Laplace transform:

$$\frac{X(s)}{A(s)} = \frac{1}{s^2 + s.\frac{D}{M_s} + \frac{K_s}{M_s}} = \frac{1}{s^2 + s.\frac{\omega_r}{Q} + {\omega_r}^2} \tag{2.2}$$

given the resonant frequency as ω_r and the quality factor as Q.

So, at low frequency where ($\omega << \omega_r$), it will be:

$$\frac{X}{A} \approx \frac{1}{{\omega_r}^2} \tag{2.3}$$

This shows that the device will get a high sensitivity with low resonant frequency because it is inversely proportional to each other.

The total of the spring constant that has been extended or retracted at a certain displacement will give a reinstating force which is relative to:

$$F = k_s x \tag{2.4}$$

In equation 2.4, K_s, the spring constant and displacement, x is proportional to force, F (Sharma, Macwan, Zhang, Hmurcik, & Xiong, 2007). There's another main principle that will show a force functioning on a mass with acceleration, Newton's second law of motion:

$$F = M_s a \tag{2.5}$$

This mass is attached to a spring and when it goes to acceleration, then by Newton's law, there will be a resultant force equal to $M_s a$.

The force will cause the mass to whichever extend or retract the spring in the limitation of:

$$F = M_s a = k_s x \tag{2.6}$$

With given acceleration, the displacement of the mass will be:

$$x = \frac{M_s a}{k_s} \tag{2.7}$$

Otherwise, the mass experienced an acceleration of:

$$a = \frac{k_s x}{M_s} \tag{2.8}$$

From there, the displacement, *x* or the acceleration, *a* can be achieved using formula above but this method only answers to the accelerations along the distance of the spring and at the single axis only. However, the same method is used to analyse data, which needs to consider each axis.

2.3.3 Accelerometer Capacitive Sensor

As mentioned earlier, capacitive sensor is commonly used type of sensor which can also turn into an actuator. It can be a high accuracy sensor with a minor temperature coefficient. It can straight away detect a variation of parameters like chemical composition, humidity, motion, proximity, electric field and other signals.

From the signal received, an electrical signal will be resultant from a point, or properties of the dielectric material. Sensors are made from conductive detecting anodes/cathodes (electrodes) in a dielectric, where detection circuits with proper amount of excitation voltages; they can change a capacitance difference into a voltage.

2.3.4 Capacitive Sensing Technique

By referring to the basic configuration in Figure 2.6, the electrodes are placed in two parallel plates. One of them is movable and the other one is fixed.

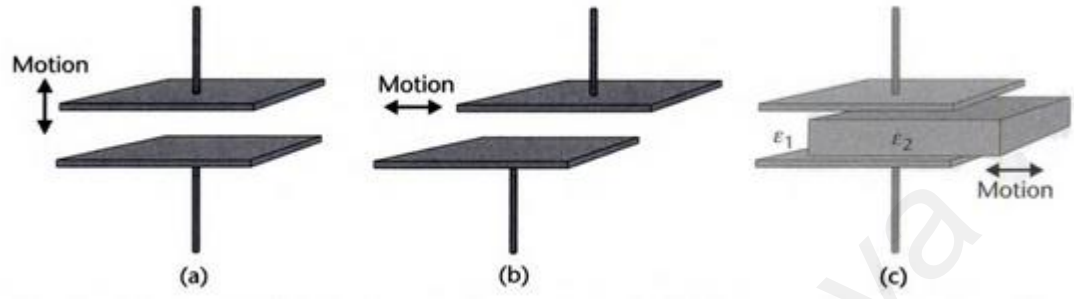

Figure 2.6 Examples of a basic capacitance model: (a) moving plate, (b) variable area, and (c) movable dielectric (Beeby, 2004)

The figure 2.6 above shows the parallel configuration that has both fixed electrode space and area of intersection. When a dielectric material is applied to the structure motion with a given dissimilar permittivity that slot in between of both electrodes, this design will be easily effected by the temperature. Then the detecting parameters of distance, area and dielectric will experience some changes that affect the signal output (Beeby, 2004). The other parallel plate configuration, transverse comb structure can rise the value of capacitance even at a small size.

As discussed previously on principle of operation, the differential capacitance is produced from the movement of the comb structure of the device has been explained. Hence, this sub-topic will elaborate in an equation form on how this capacitive MEMS works. By referring to a simple MEMS structure for differential capacitance in Figure 2.7, it shows as M_s, the fixed fingers as F_1 and F_2 and the beam as B_1 and B_2 *(Xiong, 2005).*

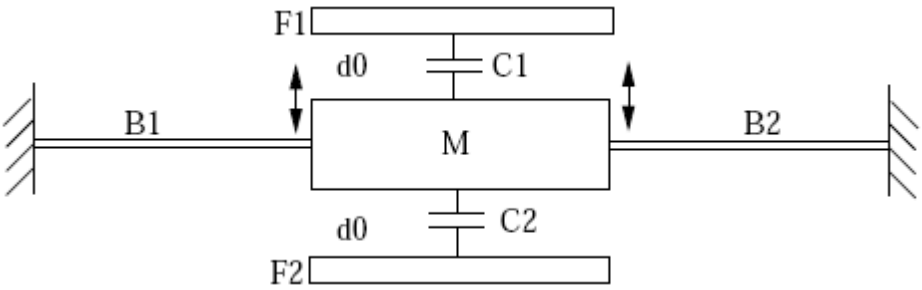

Figure 2.7 Basic schematic diagram of capacitive MEMS (Xiong, 2005)

As the moving mass is attached through the bendable beams to a substrate, this creates differential capacitance of C_1 and C_2 with the upper and lower of the fixed finger. In the stationary mode, the moving mass M_s positioned in the middle of the fingers, thus:

$$C_1 = C_2 = \frac{\varepsilon_0 . S}{d_0} \tag{2.9}$$

where dielectric constant of free space is ε_0,the joint area between mass and the fingers stated as *S*, and the stationary gap of the capacitance as d_0. The bending of beams and displacement of a moving mass M_s happen from the acceleration in the upper direction.

The displacement of x is the result of the upward movement of the moving mass M_s and given ($x << d_0$), the capacitance of C_1 and C_2 can be come out as (Xiong, 2005):

$$C_1 = \frac{\varepsilon_0 . S}{d_0 - x} \approx \frac{\varepsilon_0 . S}{d_0}(1 + \frac{x}{d_0}) \tag{2.10}$$

$$C_2 = \frac{\varepsilon_0 . S}{d_0 + x} \approx \frac{\varepsilon_0 . S}{d_0}(1 - \frac{x}{d_0}) \tag{2.11}$$

As the moving mass M_s gave a displacement of x, the voltage modulation stated as V_{mp} and V_{mn} are given to both of the fingers of F_1 and F_2 independently:

$$V_{F1} = V_{mp} = V_0.sqr(\omega.t_0) \tag{2.12}$$

$$V_{F2} = V_{mn} = -V_0.sqr(\omega.t_0) \tag{2.13}$$

where the modulation voltage amplitude presented as V_0, the frequency of the modulation voltage as ω, and time for operation as t_0.

Following the law of charge conservation, both capacitance's charges should be the same:

$$C_1(V_{F1} - V_m) = C_2(V_{F2} - V_m) \tag{2.14}$$

where the voltage level is V_m identified by the moving mass M_s. Then the equation is simplified by:

$$V_m = \left(\frac{x}{d0}\right).V_0 sqr(\omega.t) \tag{2.15}$$

Serving as a voltage divider in the middle of the upper and lower of the fingers is the moving mass M_s. The displacement x can be found by calculating the level of the voltage, V_m on the moving mass M_s. This shows the basic operation of most differential capacitive for MEMS devices (Xiong, 2005).

An electrostatic force, F_d, result from the moving mass when M experienced the voltage V_0 given to the nominal voltage $V_{nominal}$ and the fixed fingers of F_1.

$$F_d = \left(\frac{\varepsilon_0 . SV_0{}^2}{2. d_0{}^2}\right) \quad (2.16)$$

A certain threshold value cannot be exceeded by the supply voltage where the refraction is set not more than 1/3 of the gap of the capacitance, d_0. This applied to the vertical electrostatic or the moving mass will be held fixed at the fingers and ensures a short circuit.

2.3.5 Comparison of MEMS Accelerometer Design

For MEMS accelerometers, several studies on previous research have been done and Table 2.2 summarizes the comparison of the studies.

First, (Sung et al., 2014) have fabricate a gyroscope and the target was to get a resonant frequency of 9.91 kHz. In order to achieve this, they fabricate several devices with different thickness as thickness of the device is known as a major effect of the device's characteristics. From the experiments, it able to get 9.8 kHz with quality factor of 2500. From all experiments, the average resonant frequency was 10.56 kHz.

Second researcher, (Yusof, Soinb, & Noorakma, 2017) have studied the effect of beam structure of MEMS accelerometer. The study was on stress, displacement, strain and resonant frequency of the device by using COMSOL Multiphysics. For this, five different design have been compared which is from (Benichou, Benmoussa, & Ghaffour, 2013; Chunhui et al., 2012; Luo, 2013; Messina & Njuguna, 2012; Sankar, Das, & Lahiri, 2009). The experiments were setup with applied force of 50g on the devices. From the results, it can conclude that the higher stress was better for MEMS accelerometer.

(Shah, Iqbal, Shah, & Lee, 2016) has done a research on designing of a single-structure tri-axis MEMS capacitive gyroscope. The device was able to measure 3-angular velocity on a single drive. This study applied different sensing spring in which each different resulting a different frequency.

As to improve study, (Shah, Iqbal, & Lee, 2016) have design a single-structure 3-axis MEMS gyroscope with improved coupling spring. For this study, the have run a four different mode of sensing in which will give different resonant frequency.

The design of MEMS accelerometer from (Ce Zheng, 2015) with T-shape beams gives a maximum stress and displacement sensitivity. This study will be discussed in details later on for improvement and optimization by using Taguchi Method.

Finally, to obtain what is the effect of different displacement sensitivity, (Khairun Nisa, 2014) have done the studies on it. By using COMSOL Multiphysics, this experiment have varies the beam width, beam length and mass width for optimization. As the result, it can conclude that the higher value of displacement sensitivity is better for MEMS accelerometer.

Table 2.2 Summary of other researcher on MEMS accelerometer

Author	Title	Year	Objectives	Specification	Output
Jungwoo Sung, Jin Young Kim, Seyeong Seuk, Hyuckjin J Kwon, Minseo Kim, Geonhwee Kim, Geunbae Lim	A gyroscope fabrication method for high sensitive and robustness to fabrication tolerances	2014	To fabricate a gyroscope to get a targeted resonant frequency which is 9.91 kHz	1. Use a different thickness and same method of fabrication 2. This paper are more focus on fabrication of devices	1. Able to get 9.8 kHz of frequency with quality factor of 2500 2. Average resonant frequency is: 10.56 kHz
Norliyana Yusof, Norhayati Soin, Abdullah C. W Noorakma	Effect of Beam Structures on Dynamic Behaviour of Piezoresistive Accelerometer Sensor	2017	1. Presents the design and simulation analysis of MEMS piezoresistive accelerometer sensor which can be used as airbag sensors. 2. Investigate the stress, displacement, strain and resonant frequency of each structure 3. Device was tested with 50g of force	1. Simulation was done by COMSOL Multiphysics 2. Do a comparison between five different design	1. The higher stress value are better 2. With high value of stress, it may give a low value of other spec such as resonant frequency
Muhammad Ali Shah, Faisal Iqbal, Ibrar Ali Shah, Byeungleul Lee	Modal Analysis of a Single-Structure Multiaxis MEMS Gyroscope	2016	Design a single-structure tri-axis MEMS capacitive gyroscope that capable to measure 3-angular velocity on single drive	1. Use Z-shape beam for support folded coupling spring 2. This can obtain higher performance 3. Dimension of 1428 µm x 1428 µm	1. Different sensing spring will return a different frequency: - 195 µm x 4.5 µm = 13.3 kHz - 776 µm x 3.5 µm = 13.4 kHz

				4. Coupling spring to deliver desired transduction	- 776 µm x 3.5 µm (different shiffness) = 13.5 kHz - 174 µm x 3 µm = 13.5 kHz
Muhammad Ali Shah, Faisal Iqbal, Byeungleul Lee	Design and Analysis of a Single-Structure Three-Axis MEMS Gyroscope with Improved Coupling Spring	2016	1. Design 3-axis MEMS gyroscope 2. Contain unique and simple coupling spring 3. Measured the resonant frequency	Four modes of sensing used to measure the resonant frequency: 1. Drive mode 2. Pitch sensing mode 3. Roll sensing mode 4. Yaw sensing mode	1. Drive mode give 15206 Hz 2. Pitch sensing give 15215 Hz 3. Roll sensing give 15320 Hz 4. Yaw sensing give 15595 Hz
Ce Zheng, Xingguo Xiong, Junling Hu	COMSOL simulation of a dual-axis MEMS accelerometer with T-shape beams	2015	1. Design a 2-axis MEMS accelerometer with T-shape beams 2. Simulate the displacement sensitivity and stress of device	1. Have two T-shape beams: X-beam and Y-beam 2. Applied a force of 50g with gravity of 9.8 m/s^2	Displacement Sensitivity: X-axis: 0.0051578 µm/g Y-axis: 0.0026694 µm/g Stress: X-axis: 4.5594 x 10^6 Pa Y-axis: 2.5348 x 10^6 Pa
Khairun Nisa Khamil	Design and analysis of MEMS capacitive accelerometer with optimized sensitivity	2013	Optimize MEMS accelerometer structure by enhancing the device sensitivity	1. Design the device using COMSOL Multiphysics 2. Measure the displacement sensitivity 3. Do an optimization to get the optimum displacement sensitivity	1. Varies of beam width, beam length and mass width will give the different value of displacement sensitivity 2. The higher value of displacement sensitivity are better for the device

2.4 Selection of Model Structure

2.4.1 Model Structure

As mention on previous sub-topic, this report will be focusing on improvement and optimization of MEMS accelerometer that have been design by (Ce Zheng, 2015). Figure 2.8 shows the design of MEMS accelerometer. The device has two T-shape beams and both are connected to a moveable mass. It was designed symmetric vertically and horizontally.

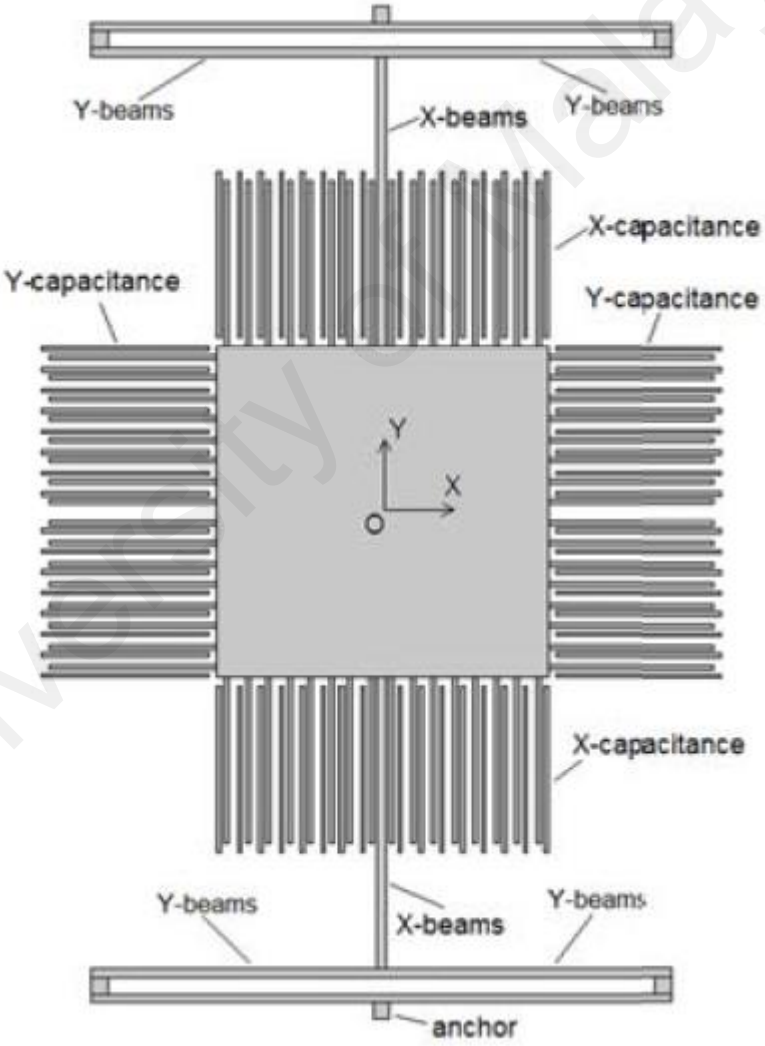

Figure 2.8 Structural diagram of dual-axis MEMS accelerometer (Ce Zheng, 2015)

For each T-shape beam, it consists of one straight beam and two folded beams. These beams are connected between the anchors and the central mass. The device also designed with eight groups of moveable fingers at all four side of device.

Table 2.3 shows the size of all parameters of this device. These parameters are important in order to get the similar result to continue the optimization process. All simulation from designing and analysis, it was done by using COMSOL Multiphysics while the optimization was done by using Taguchi Method. Polysilicon is used as the material of this device and it can be applied at COMSOL Multiphysics. The thickness of the device was set as 4 µm.

Table 2.3 Design parameters of MEMS accelerometer(Ce Zheng, 2015)

Components	**Amount**	**Length (µm)**	**Width (µm)**
Central Mass	1	800	800
Moveable Fingers	64 (8 x 8)	400	10
Fixed Fingers	64	400	10
Folded Beam Segments	8	700	20
Straight Beams	2	700	20
Anchors	2	40	40

2.4.2 Model Device Analysis

The simulation was all done by using COMSOL Multiphysics and it are using the Solid Mechanics physics and Electromechanics physics. For this project, the physics used only with Solid Mechanics as it was enough to simulate the maximum stress as well as displacement sensitivity of X-axis and Y-axis. The details of this selected physics will be discussed on next sub-topics on Finite Elements Modelling tools.

The force will be applied on certain part of the device and the measurement of stress and displacement sensitivity will discussed. Force will depending on 50 g analysis with applied of gravity acceleration unit of 1g = 9.8m/s^2. All of this will further discussed on chapter 3 of methodology.

2.4.3 Maximum Stress and Displacement Sensitivity Results

(Ce Zheng, 2015) has concluded the value of stress and displacement sensitivity for both y-axis beam and x-axis beam. The summary of result was shown in Table 2.4.

Table 2.4 Stress and sensitivity result (Ce Zheng, 2015)

Beam	Stress (Pa)	Displacement Sensitivity (µm/g)
X-axis	4.5594 x 10^6	0.0051578
Y-axis	2.5348 x 10^6	0.0026694

The objective of this report was to get the optimal stress and displacement sensitivity for both beams by using a Taguchi Method of optimization and the value must be larger than these results.

2.5 Simulation Tools

2.5.1 MEMS Model

In analysing the MEMS devices, it is a challenging job to design and develop this miniature part to see how it could work, and function accurately. Each component such as spring, the folded beams, mass and other micro parts which are fabricated on the same chips must be precise to give maximum stress and vibration to sufficiently archive

its mechanical tasks. Thus, this accelerometer is required to be evaluated meticulously such as its mechanics, stress, displacement, electrical and others.

The best way to evaluate this MEMS model is through simulation. The effect of numerous design constraints that can be applied and the performances of the device can be forecasted without having to fabricate the device. By using the simulation, any changes can be made directly without any fabrication hassle which make it easier to use and understood.

Finite Element Modelling (FEM) are selected in this study because this method approaches from mechanical engineering point of view where the mechanical reactions to forces, motion and predicted. This method also preferable because it is closer to the real device. The tools selected was COMSOL Multiphysics as it is also used by (Ce Zheng, 2015) to complete the research.

2.5.2 COMSOL Multiphysics

COMSOL Multiphysics can be used to design and model the microelectromechanical systems (MEMS) device especially in the micro dimension which can predict the outcome of any solid circumstances in its process virtually either in two or three dimension structure. MEMS Module in COMSOL Multiphysics offers user interfaces with modelling tools, physics interfaces, and also provides variety of the coupled physics and damping conditions in MEMS model.

The MEMS module consists of studies in the stationary and transient fields, such as time dependent, eigenfrequency, modal and frequency response studies and parametric. From there, a simple lumped parameter extraction can be made to find the capacitance, impedance and admittance. Finite Element tool simulation and design

process begin with the illustration of device geometry in both two and three dimensional solid models, meshing the geometry and then evaluating the device.

The Structural Mechanics Module solves problems in the fields of structural and solid mechanics, adding special physics interfaces for modelling shells and beams, for example. The physics interfaces in this module are fully multiphysics enabled, making it possible to couple them to any other physics interfaces in COMSOL Multiphysics or the other modules. Available physics interfaces included many of items such as Solid mechanics for 2D plane stress and plane strain, axial symmetry, and 3D solids, Piezoelectric modelling, beams in 2D and 3D, Euler theory, truss and cable elements, shells and plates and membranes. The module's study capabilities include static, eigenfrequency, time dependent (transient), frequency response, buckling, and parametric studies.

Next step is to choose the intended physic interface analysis that comprises predefined models and user interfaces already set up with equations and variables for specific areas of physics such as in Table 2.5.

Table 2.5 Physics group in Model Wizard (Multiphysics, 2013)

Physics	**Description**
Static Analysis	In a static analysis the load and constraints are fixed in time.
Eigenfrequency Analysis	An eigenfrequency analysis finds the damped or undamped eigenfrequencies and mode shapes of a model. Sometimes referred to as the free vibration of a structure. Pre-stress effects can be taken into account.
Transient Analysis	A transient analysis finds the transient response for a time-dependent model, taking into account mass, mass moment of inertia. The transient analysis can be either direct, or using a modal solution.
Frequency Response	A frequency response analysis finds the steady-state response from harmonic

Analysis	loads. The frequency-response analysis can be either direct, or using a modal solution. Effects of pre-stress can be included.
Parametric Analysis	A parametric analysis finds the solution dependence due to the variation of a specific parameter, which could be, for instance, a material property or the position of a load.
Thermal Stress	In a transient thermal stress study, the program neglects mass effects, assuming that the time scale in the structural mechanics problem is much smaller than the time scale in the thermal problem.
Large Deformations	enable the geometric nonlinearity for the Linear Elastic Material under all structural mechanics interfaces except the Beam interface. The engineering strain is then replaced with the Green-Lagrange strain and the stress with the second Piola-Kirchhoff stress. Such material is suitable to study deformations accompanied by possible large rotations but small to moderate strains in the material, and it is sometimes referred to as Saint Venant-Kirchhoff hyperelastic material. To solve the problem, the program uses a total Lagrangian formulation.
Displacement	A condition where the displacements are prescribed in one or more directions to the geometric entity.

2.6 Optimization Process

2.6.1 Introduction of Optimization

Optimization can be described as maximizing or minimizing of some set. It was often representing a range of choices available in some certain situation. For MEMS, there are several parameters can be modified to get the optimal results such as thickness, length and width of the device, material used of the device and much more other possibilities.

Nowadays, there are a lot of optimization methods such as Taguchi Method, trial and error, Local Kalman Filter, Mathematical Methods and many more. For this report, Taguchi Method will be selected as the optimization method.

All of the optimization process will be done on three parameters which are length, width and thickness as these parameters was studies by (Ce Zheng, 2015; Kaya, Shiari, Petsch, & Yates, 2011) and will resulting most effect on maximum stress and displacement sensitivity. For length and width, it will be done by modify the beam according to which axis it was and the thickness will affected the whole device. These parameters was selected due to the big margin can be obtained during analysis.

2.6.2 Taguchi Method

Taguchi Method is known as one of a systematic approach for optimization of various process parameters necessary to study their combined effects with regard to device performance. Taguchi defines the quality of a product in terms of the loss imparted by the product to the society from the time the product is shipped to the customer(Ghani, Choudhury, & Hassan, 2004). Some of these losses are due to deviation of the product's functional characteristic from its desired target value, and these are called losses due to functional variation. The uncontrollable factors which cause the functional characteristics of a product to deviate from their target values are called noise factors, which can be classified as external factors (e.g. temperatures and human errors), manufacturing imperfections (e.g. unit to unit variation in product parameters) and product deterioration. The overall aim of quality engineering is to make products that are robust with respect to all noise factors.

The Taguchi method used the conceptual signal-to-noise (S/N) approach, as express below by visually identifying the significant factors:

Nominal is best (NIB): $S/N = 10log\frac{\bar{y}}{{s_y}^2}$ (2.17)

Smaller the best (STB): $S/N = -10log\frac{1}{n}(\sum y^2)$ (2.18)

Larger the best (LTB): $S/N = -10log\frac{1}{n}(\sum\frac{1}{y^2})$ (2.19)

Where ȳ is the average of the simulation data, s_y^2 is the variance of *y*, *n* is the number of observations, and *y* is the simulation data.

$$Variance: {s_y}^2 = \frac{\sum_{i=1}^{n}(y_i - \bar{y})}{n-1} \quad (2.20)$$

$$Average: \bar{y} = \frac{y_0 + y_1 + \cdots + y_2}{n} \quad (2.21)$$

For this project, as research done by (Yusof et al., 2017) and (Khairun Nisa, 2014) both axis analysis will used Larger the best (LTB) since the larger stress and displacement sensitivity was the better for device.

The details on step-by-step of applying a Taguchi method will be more described in Chapter 3 Methodology.

CHAPTER 3 : METHODOLOGY

3.1 Introduction

This chapter will present the methodology of completing this project. In general, the method start with redesign the device by using COMSOL Multiphysics and get the expected results as done by (Ce Zheng, 2015), followed by doing the same design but additional changes in the three parameters which is length, width and thickness of device. This step will be done for both X-axis and Y-axis. After complete, optimization by using Taguchi method will be done and finally, the result will be discussed and analysed.

3.2 Flow Chart of Overall Project

Figure 3.1 shows the flow chart of overall projects and each of it will be discussed in details in this chapter.

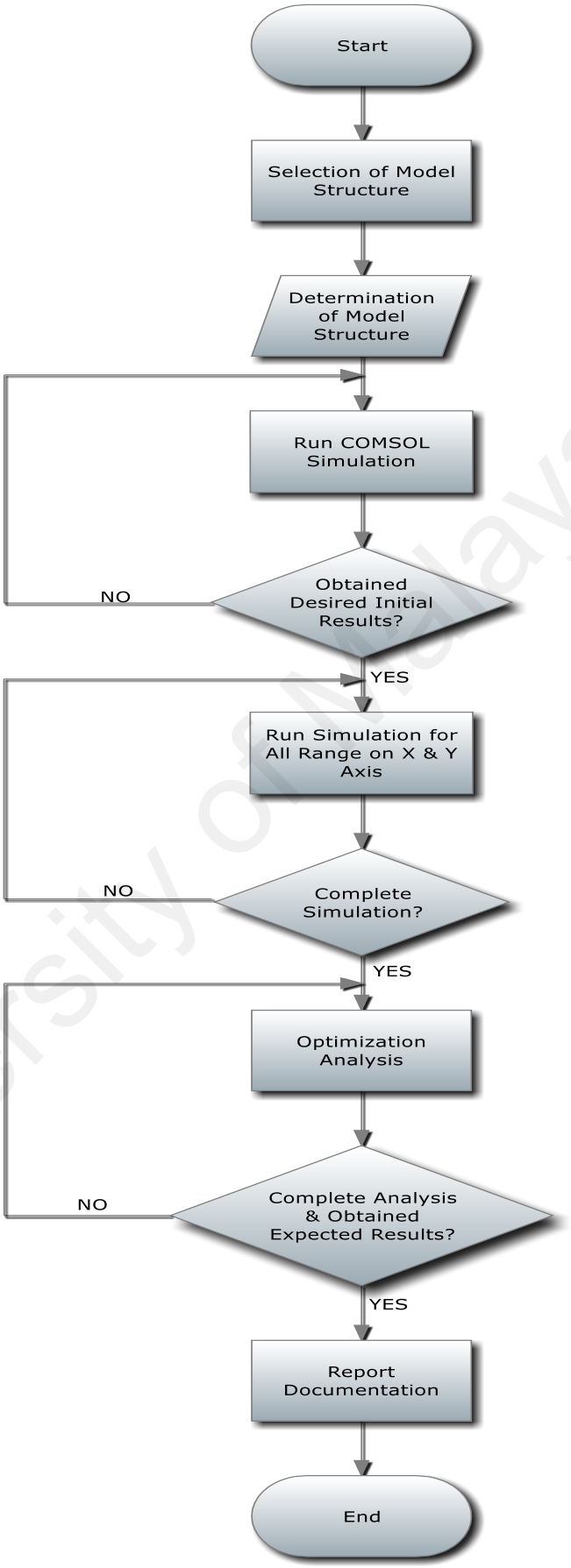

Figure 3.1 Flow chart methodology of the overall project

3.3 Selection of Model Structure

As discussed in section 2.3 of this report, (Ce Zheng, 2015) designed were selected as researcher were able to study the maximum stress and displacement sensitivity of MEMS accelerometer. These two results have been declare as important for lower limb exoskeleton as discussed in section 2.2. Figure 3.2 shows the dual axis mode with T-shape beam capacitance accelerometer and the study was to see effect of this T-shape beam on the device.

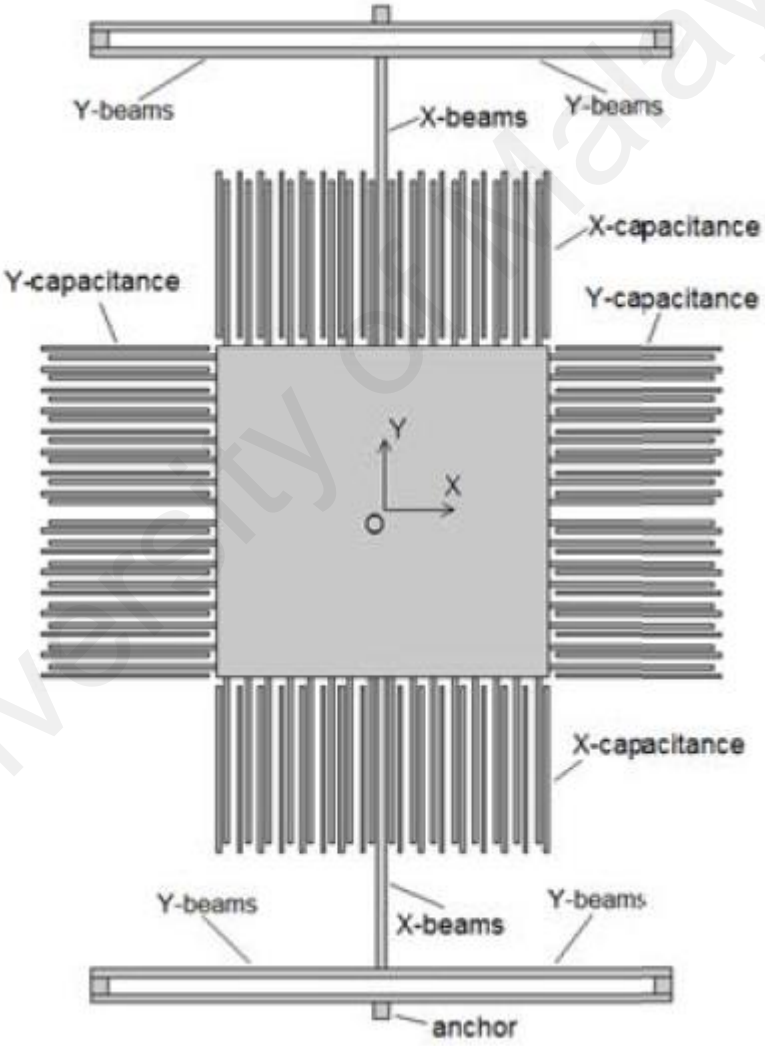

(a)

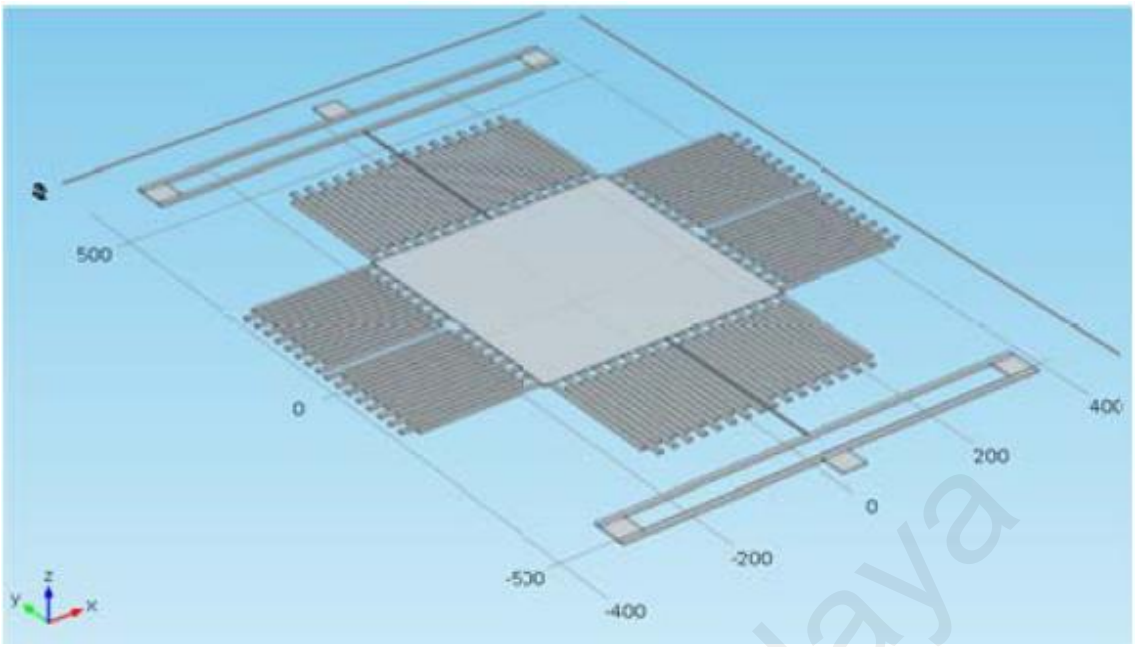

(b)

Figure 3.2 Design of device: (a) top view, (b) side view (Ce Zheng, 2015)

By using this published model, the model structure, model physic in the simulation and its boundary condition, material properties and some of dimension are determined. Published model is used in this research project to verify the MEMS model built with COMSOL Multiphysics.

3.4 Determination of Design Parameters

The design parameters and material properties needed to construct and model the structure were taken from the original model of (Ce Zheng, 2015).

Table 3.1 Structure label and dimension

Components	Amount	Length (μm)	Width (μm)
Central Mass	1	800	800
Moveable Fingers	64 (8 x 8)	400	10
Fixed Fingers	64	400	10

Folded Beam Segments	8	700	20
Straight Beams	2	700	20
Anchors	2	40	40

In addition, table 3.2 shows other parameters that are calculated by length and width of central mass divided with number of fingers. By this, the gap between fingers is almost equal between each other same goes the gap between fixed and moveable fingers.

Table 3.2 Dimension declared for this study

Parameters	**Dimension**
Gap between each moveable fingers	45 µm
Gap between each moveable fingers with fixed capacitance fingers	5 µm
Gap between central mass with fixed capacitance fingers	10 µm
Gap between X-beam with first moveable finger	50 µm
Gap between middle fingers on left and right side of central mass	120 µm

(Ce Zheng, 2015) have used polysilicon as the material of the MEMS accelerometer and table 3.3 shows the properties that will be used for this study.

Table 3.3 Material properties

Material Properties	**Label**	**Values**
Density	ρ	2320 kg / m^3
Young's Modulus of polysilicon	E	160 x 10^6 Pa
Poisson's ratio	v	0.22
Electric constant	ε_o	8.85 x 10^{12} (F/m)
Dielectric permittivity of polysilicon	ε_r	11.9

3.5 COMSOL Multiphysics Simulation

The simulation is conducted using COMSOL Multiphysics 4.4 trial version. The objective for the simulation is to obtain maximum stress and displacement sensitivity of the device. Simulation was started with geometry modelling of the structure. The structure is built based on the simulation condition of device characteristics in the Table 3.1, 3.2 and 3.3. The values in Table 3.3 are inserted in the Material Overview tab while the structure dimension values and design specification are inserted in Global Definition of Parameter tab. The simulations were performed using the application mode of Solid Mechanics in the MEMS module. Figure 3.3 shows the flow chart for the simulation in COMSOL Multiphysics.

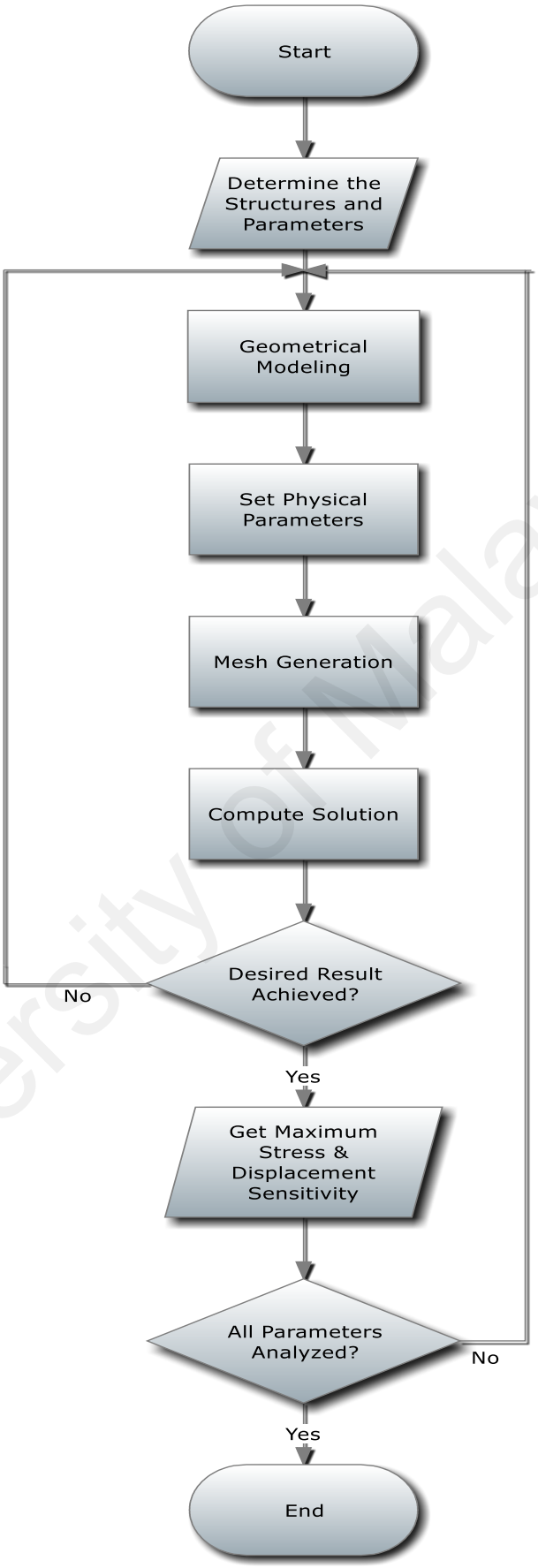

Figure 3.3 Flow chart for MEMS accelerometer simulation using COMSOL Multiphysics

After the design was completed (see Figure 3.4), next step is to run simulation on X-axis and Y-axis. For X-axis simulation, the force was applied on the central mass (Figure 3.5(a)) while four beam joints will be applied with force for Y-axis simulation (Figure 3.5(b)). Equation 3.1 shows the formula of total force to be applied. The 50g of gravity was applied with unit gravity acceleration of 1g = 9.8 m/s^2.

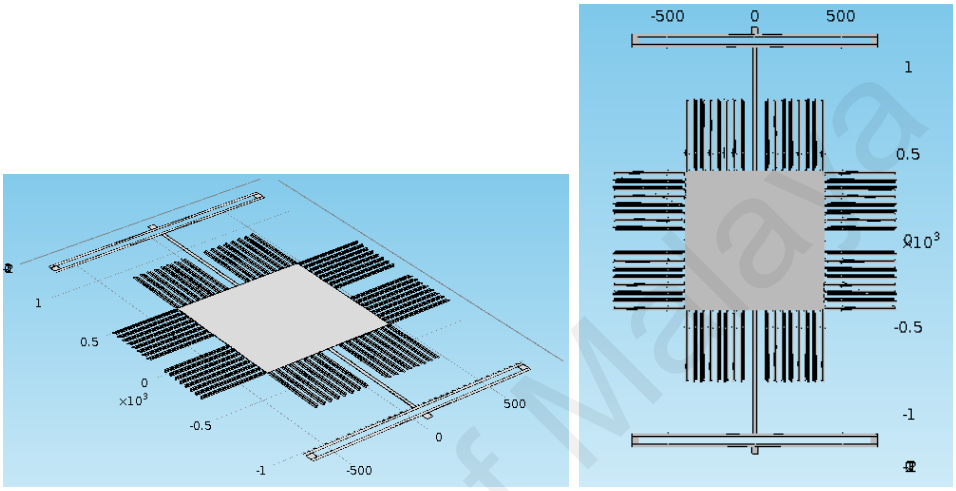

Figure 3.4 Completed design by COMSOL

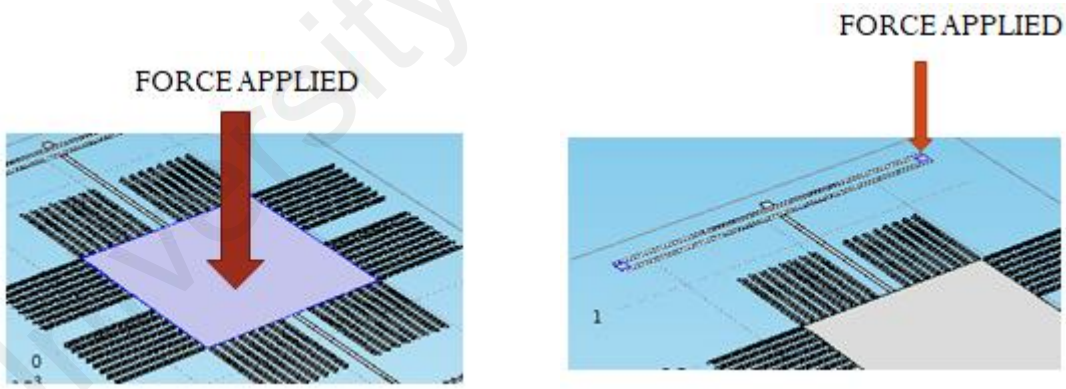

(a) (b)

Figure 3.5 Force applied for: (a) X-axis simulation, (b) Y-axis simulation

$$F = mA \tag{3.1}$$

Where F is total force, m mass which is density of material (ρ) multiply with volume and A is speed (50g x 9.8 m/s^2).

3.6 Parameters of X-axis and Y-axis Simulations

After completing the design of initial device and get results as (Ce Zheng, 2015), next is to do an optimization with five differences in variation and the variation was set with ±5%, ±10%, ±15%, ±20%, and ±25% of original value. This variation will be applied on three parameters which is length and width of each beam and thickness of the whole device. These three parameters have been identify as the most affected parameters for maximum stress and displacement sensitivity of this kind of device as research done by (Ce Zheng, 2015; Kaya, Shiari, Petsch, & Yates, 2011; Yusof, Soinb, & Noorakma, 2017). Table 3.4 and table 3.5 shows the value of parameters with variation that have been setup for X-axis and Y-axis. As we can see, at 25% of variation, the thickness of maximum device is 5 µm which is declared as maximum thickness as mention by (Kaya et al., 2011)

Table 3.4 Parameters variant for X-axis experiment setup

Difference	Factor	Level 0, Least	Level 1, Intermediate	Level 2, Largest
± 5%	Length	665 µm	700 µm	735 µm
	Width	19 µm	20 µm	21 µm
	Thickness	3.8 µm	4 µm	4.2 µm
± 10%	Length	630 µm	700 µm	770 µm
	Width	18 µm	20 µm	22 µm
	Thickness	3.6 µm	4 µm	4.4 µm

± 15%	Length	595 µm	700 µm	805 µm
	Width	17 µm	20 µm	23 µm
	Thickness	3.4 µm	4 µm	4.8 µm
± 20%	Length	560 µm	700 µm	840 µm
	Width	16 µm	20 µm	24 µm
	Thickness	3.2 µm	4 µm	4.8 µm
± 25%	Length	525 µm	700 µm	875 µm
	Width	15 µm	20 µm	25 µm
	Thickness	3 µm	4 µm	5 µm

Table 3.5 Parameters variant for Y-axis experiment setup

Difference	Factor	Level 0, Least	Level 1, Intermediate	Level 2, Largest
± 5%	Length	1330 µm	1400 µm	1470 µm
	Width	19 µm	20 µm	21 µm
	Thickness	3.8 µm	4 µm	4.2 µm
± 10%	Length	1260 µm	1400 µm	1540 µm
	Width	18 µm	20 µm	22 µm
	Thickness	3.6 µm	4 µm	4.4 µm
± 15%	Length	1190 µm	1400 µm	1610 µm
	Width	17 µm	20 µm	23 µm
	Thickness	3.4 µm	4 µm	4.8 µm
± 20%	Length	1120 µm	1400 µm	1680 µm
	Width	16 µm	20 µm	24 µm
	Thickness	3.2 µm	4 µm	4.8 µm

± 25%	Length	1050 μm	1400 μm	1750 μm
	Width	15 μm	20 μm	25 μm
	Thickness	3 μm	4 μm	5 μm

3.7 Optimization Using Taguchi Method

In chapter 2, a brief introduction of Taguchi Method already discussed. In this sub-topic will discuss step-by-step to complete an optimization using Taguchi Method. This project consists of three parameters that needed to be varies which are: length and width of beams and thickness of device. As there are three parameters, the experiments have run simulation for total of 27 times by following the factor A, B and C as shown in Appendix C.

After complete the results, next is to calculate a conceptual signal-to-noise (S/N) approach an as discussed in chapter 2, larger the best (LTB) calculation will be used and it follows equation 2.18. Next step is to draw the S/N graph for each value measured which in this project are displacement sensitivity and maximum stress. After getting the graph, next is to identify which interaction give the highest maximum-minimum different and this different will tell us that this two parameter's interaction give the highest change of difference.

Next step is to draw the two-way table and from this table, the highest S/N ratio of each parameter will be identify and it will declared as the optimal value for these two parameters. Later, the third optimal parameter will be identified by check the highest S/N ratio of that particular parameter.

Last but not least, in order to confirm the results that been obtained in above step, Pareto ANOVA method will be applied by completed the table as shown in

Appendix C. Then, from the graph, it can confirm either the optimal result is right or not. In summary, figure 3.6 shows the flow chart of these Taguchi method process.

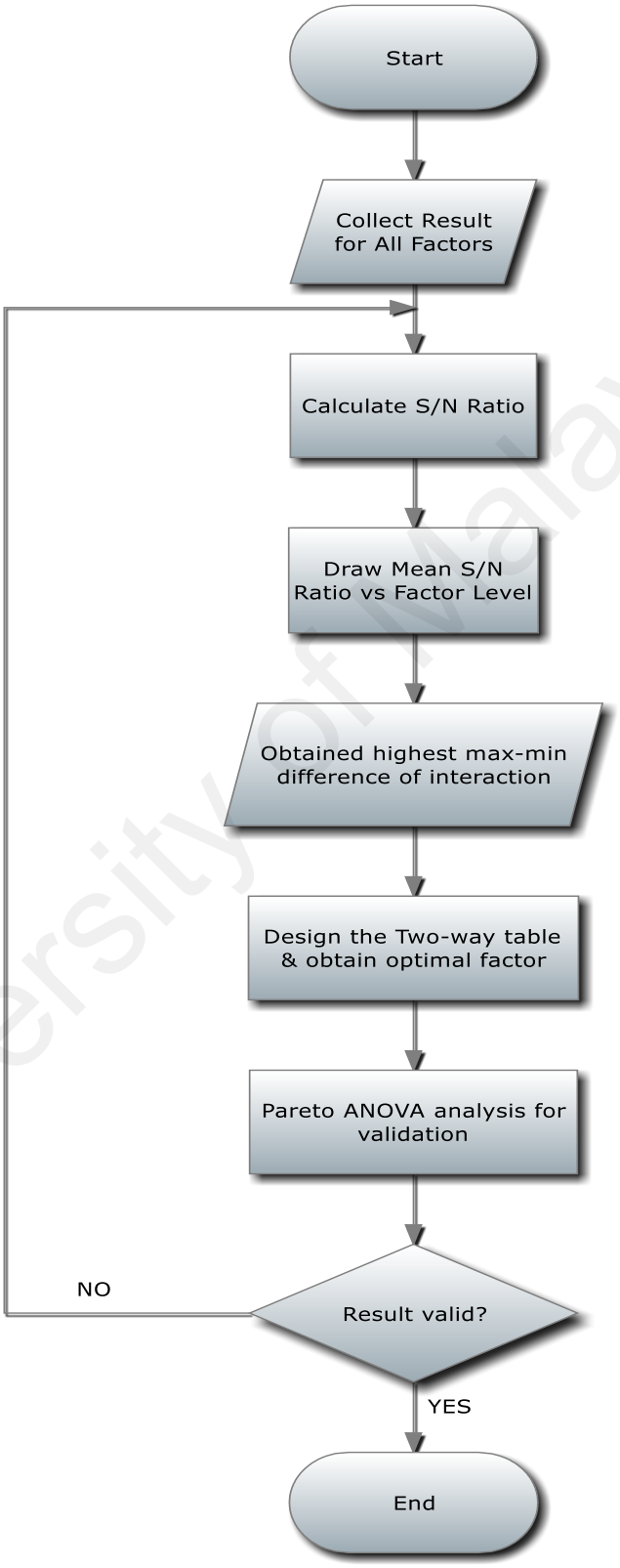

Figure 3.6 Flow chart for Taguchi method

CHAPTER 4 : RESULTS AND DISCUSSION

4.1 Introduction

This chapter will present and discuss the simulation results of the projects. First, COMSOL Multiphysics simulation results of the selection model as (Ce Zheng, 2015) will be discussed. After that, for five different variation of ±5%, ±10%, ±15%, ±20%, and ±25% of the length and width of beam and thickness of device will be simulate also by using COMSOL Multiphysics. This step will be applied for both X-axis and Y-axis analysis. After obtaining the value of maximum stress and displacement sensitivity, Taguchi method analysis will be applied for optimization.

4.2 COMSOL Multiphysics Simulation for Selected Model Structure

Figure 4.1 shows the design of selected model structure (Ce Zheng, 2015) by using COMSOL Multiphysics. Maximum stress and displacement sensitivity will be obtained by using this setup and the results must be similar with research done by (Ce Zheng, 2015).

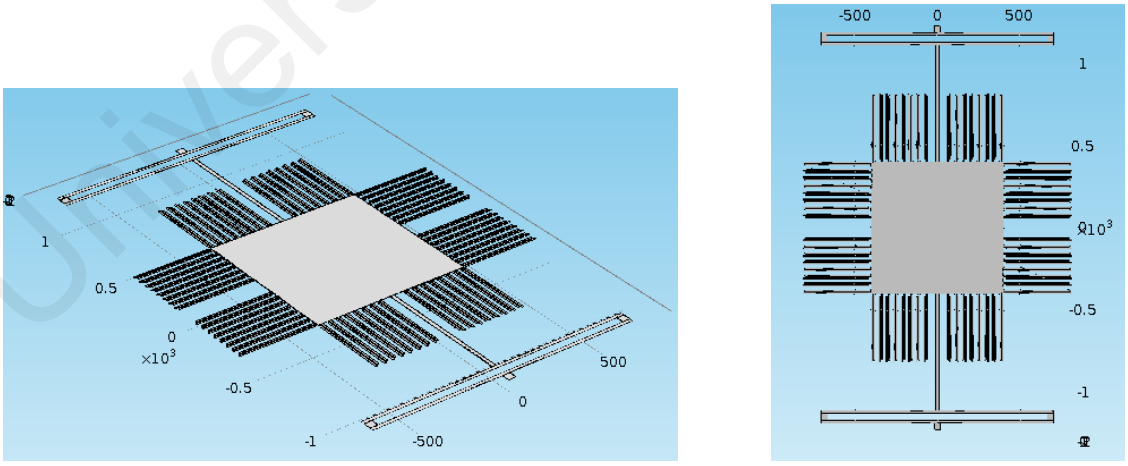

(a) (b)

Figure 4.1 Design of the device by using COMSOL Multiphysics. (a) from x-y-z view, (b) x-y top view

4.2.1 X-axis Results for Selected Model Structure

By using the setup as discussed on chapter 3 of methodology, figure 4.2 and figure 4.3 shows the maximum stress and displacement sensitivity simulation result from COMSOL Multiphysics. To summarize the result, table 4.1 shows the value of maximum stress and displacement sensitivity of the simulation and comparison with the reference results.

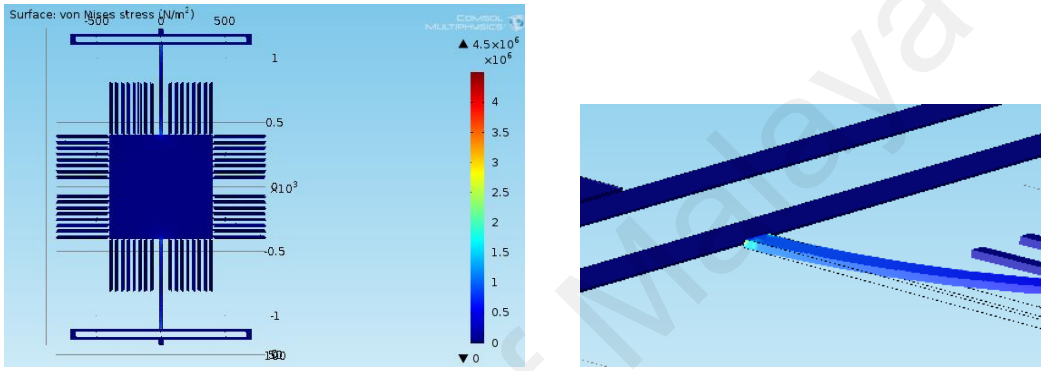

(a) (b)

Figure 4.2 Simulation results for the stress of X-axis. (a) simulation view, (b) the maximum stress at the X-beam

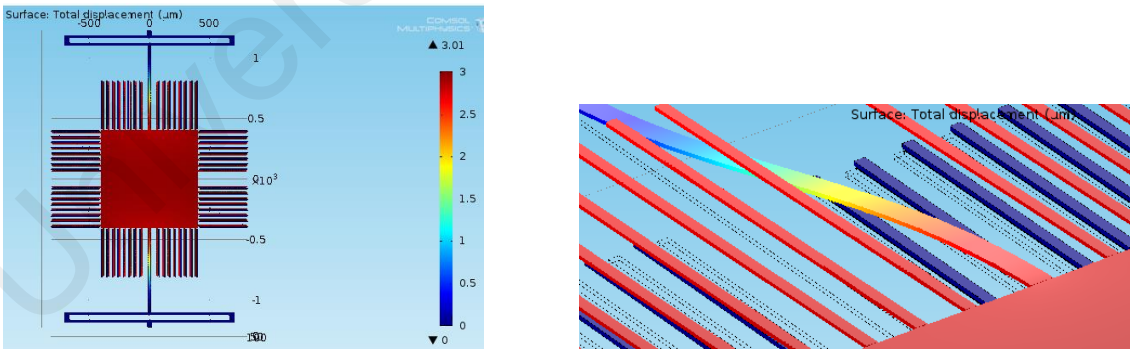

(a) (b)

Figure 4.3 Displacement simulations for X-axis. (a) simulation view, (b) the maximum displacement at the X-beam

Table 4.1 Comparison of simulation results with the (Ce Zheng, 2015) result for X-Axis

Simulation	**Result**	**Reference**	**Percentage of Difference**
Maximum Stress (Pa)	4.49611×10^6	4.5594×10^6	1.388 %
Displacement Sensitivity (μm/g)	0.00614	0.0051578	19.04 %

Based on this initial simulation results, the difference for maximum stress was very small which is 1.388% of difference. Meanwhile, the displacement sensitivity result shown a little bit higher of difference which is 19.04%.

Previously in section 3.4 of this report, table 3.2 explained other parameters that are calculated by length and width of central mass divided with number of fingers. In this study, the distance between each combs was declared as a variable parameters and for this study, the distance applied was shown in table 3.2. This distance between combs was different compared research designed by (Ce Zheng, 2015) as it was a variable parameters and this will cause the difference as shown on table 4.1. Figure 4.4 show how the differential capacitance sensing for acceleration along X-axis that gives this differences (Ce Zheng, 2015).

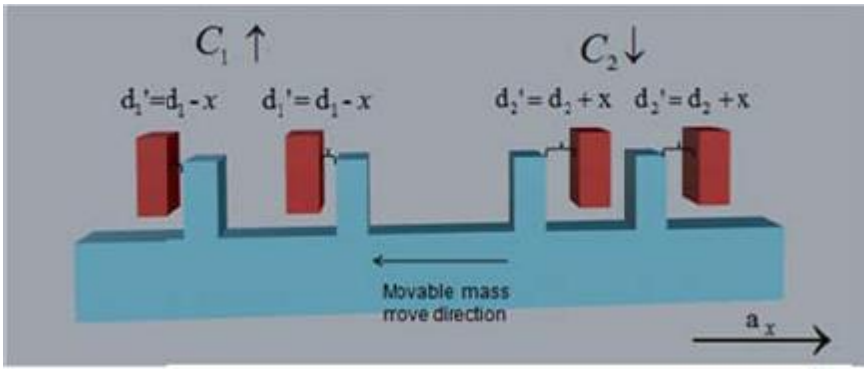

Figure 4.4 Differential capacitance sensing for acceleration along X-axis (Ce Zheng, 2015)

For the dual-axis MEMS accelerometer with T-shape beams, the left capacitance gap must be equal to the right capacitance gap ($d_1=d_2=d_0$) for the X-capacitance. That make the left X-capacitance equals to the right X-capacitance ($C_1=C_2=C_{x0}$). When there is acceleration along the X-axis direction, due to inertial force, the moveable fingers move toward left by displacement of x, then: $d_1'=d_0-x$, $d_2'=d_0+x$, the X-capacitance change is

$$\Delta C_x = C_1' - C_2' \approx 2\Delta C_1 = 2\frac{N_x \varepsilon S}{d_0}.(\frac{x}{d_0}) \tag{4.1}$$

where N_x is the number of X-differential capacitance groups, ε is permittivity of air, S is the overlap area between a moveable finger and its left (or right) fixed finger ($S=t$ x L_{ov}, in its t is the device thickness and L_{ov} is the overlap length between moveable and fixed finger), d_0 is the static capacitance gap of X-capacitance (Ce Zheng, 2015). This proves that the gap between combs gives differences on device's maximum stress and displacement sensitivity.

4.2.2 Y-axis Results for Selected Model Structure

Similar method applied in 4.2.1, the Y-axis analysis will be done in the same way. Figure 4.5 and Figure 4.6 shows the maximum stress and displacement sensitivity

simulation result of Y-axis from COMSOL Multiphysics. To summarize the result, table 4.2 shows the value of maximum stress and displacement sensitivity of the simulation and comparison with the (Ce Zheng, 2015) results.

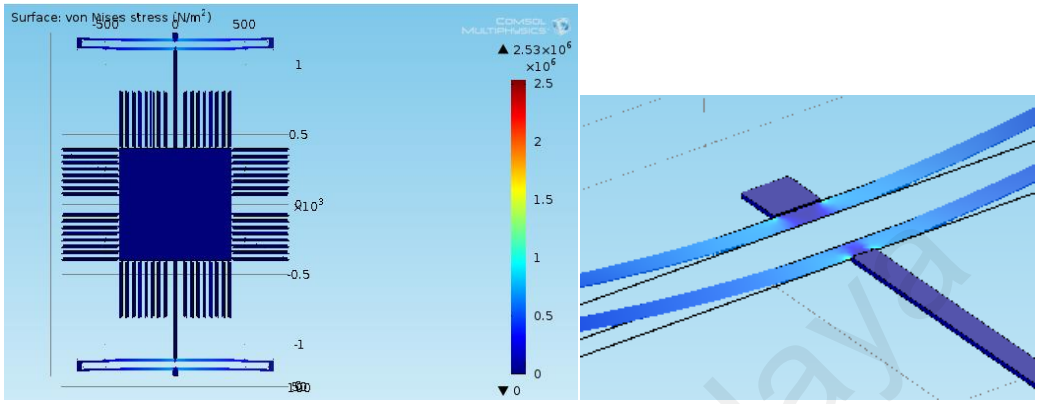

(a) (b)

Figure 4.5 Simulation results for the stress of Y-axis. (a) simulation view, (b) the maximum stress at the Y-beam

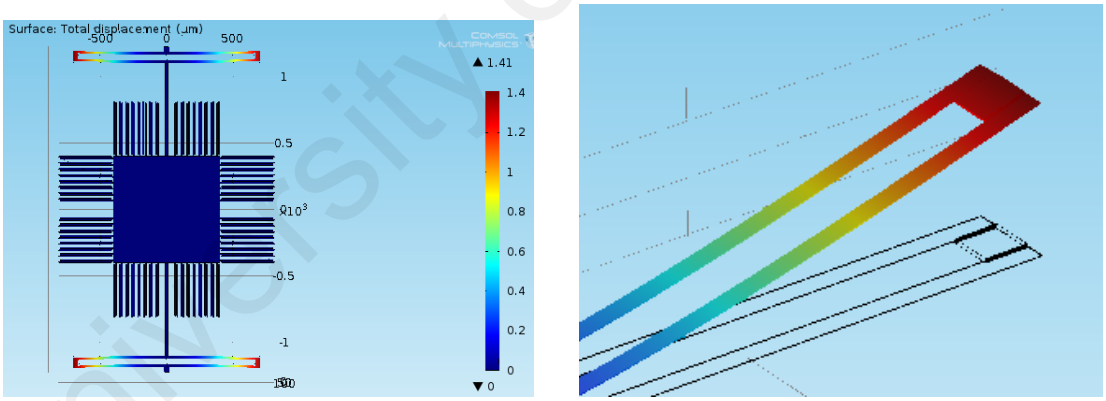

(a) (b)

Figure 4.6 Displacement simulations for Y-axis. (a) simulation view, (b) the maximum displacement at the Y-beam

Table 4.2 Comparison of simulation results with the (Ce Zheng, 2015) result for Y-Axis

Simulation	**Result**	**Reference**	**Percentage of Difference**
Maximum Stress (Pa)	2.53311×10^6	2.5348×10^6	0.067 %
Displacement Sensitivity (µm/g)	0.002873	0.0026694	7.627 %

Based on this initial simulation results, the difference for maximum stress was very small which is 0.067% of difference. Meanwhile, the displacement sensitivity give a little bit higher of difference which is 7.627%.

As the analysis in 4.2.1 for X-axis, the gap between combs might be different compared to research done by (Ce Zheng, 2015) and it gives the different results as table 4.2. Figure 4.7 show how the differential capacitance sensing for acceleration along Y-axis that will make this small different of result.

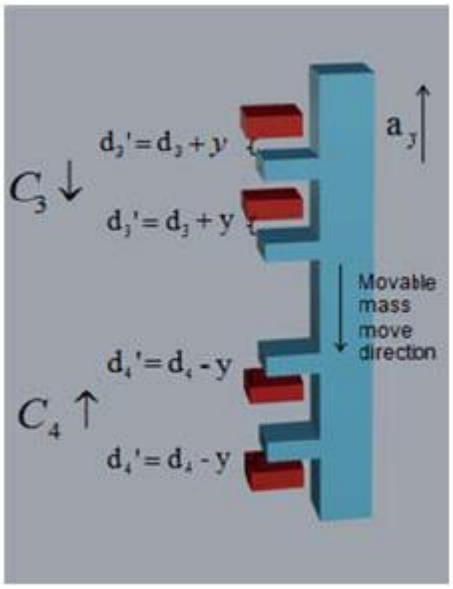

Figure 4.7 Differential capacitance sensing for acceleration along Y-axis (Ce Zheng, 2015)

The top capacitance gap is equal to the bottom capacitance gap (d_3=d_4=d_0) for Y-capacitance. As the result, the top Y-capacitance equals to bottom Y-capacitance (C_3=C_4=C_{y0}). When there is acceleration along Y-axis direction, assume moveable fingers move toward bottom by displacement y due to inertial force. As a result, d_3'=d_0+y, d_4'=d_0-y, the Y-differential capacitance charge is

$$\Delta C_y = C_3' - C_4' \approx 2\Delta C_3 = 2\frac{N_y \varepsilon S}{d_0}.(\frac{y}{d_0}) \tag{4.2}$$

where N_y is the number of Y-differential capacitance groups, S is the overlap area between a moveable finger and its top (or bottom) fixed finger, d_0 is the static capacitance gap of Y-capacitance (Ce Zheng, 2015).

4.3 Optimization for X-axis of MEMS Accelerometer

4.3.1 Parameter of X-axis Analysis

As discussed in section 3.6, five different values for three parameters which is length and width of beam and thickness of device will be applied for optimization and analysis on maximum stress and displacement sensitivity of device. These three parameters have been identified as the most affected parameters for maximum stress and displacement sensitivity of this kind of device as research done by (Ce Zheng, 2015; Kaya, Shiari, Petsch, & Yates, 2011; Yusof, Soinb, & Noorakma, 2017). The parameter values for these simulation were shown in Table 4.3 below.

Table 4.3 Parameters variant for X-axis for each variation

Difference	Factor	Level 0, Least	Level 1, Intermediate	Level 2, Largest
± 5%	Length	665 µm	700 µm	735 µm
	Width	19 µm	20 µm	21 µm
	Thickness	3.8 µm	4 µm	4.2 µm
± 10%	Length	630 µm	700 µm	770 µm
	Width	18 µm	20 µm	22 µm
	Thickness	3.6 µm	4 µm	4.4 µm
± 15%	Length	595 µm	700 µm	805 µm
	Width	17 µm	20 µm	23 µm
	Thickness	3.4 µm	4 µm	4.8 µm
± 20%	Length	560 µm	700 µm	840 µm
	Width	16 µm	20 µm	24 µm
	Thickness	3.2 µm	4 µm	4.8 µm
± 25%	Length	525 µm	700 µm	875 µm
	Width	15 µm	20 µm	25 µm
	Thickness	3 µm	4 µm	5 µm

4.3.2 Optimization Results in X-axis

For each variation of parameters will be simulated by using COMSOL Multiphysics and Taguchi method will be applied for optimization for X-axis. This topic will only show the graph and important results for the experiments. All detailed data were shown in Appendix A of this report.

4.3.2.1 Optimization with Variation of ±5% for X-axis

Figure 4.8 shows the graph of Mean S/N ratio at ±5% variation of parameters value.

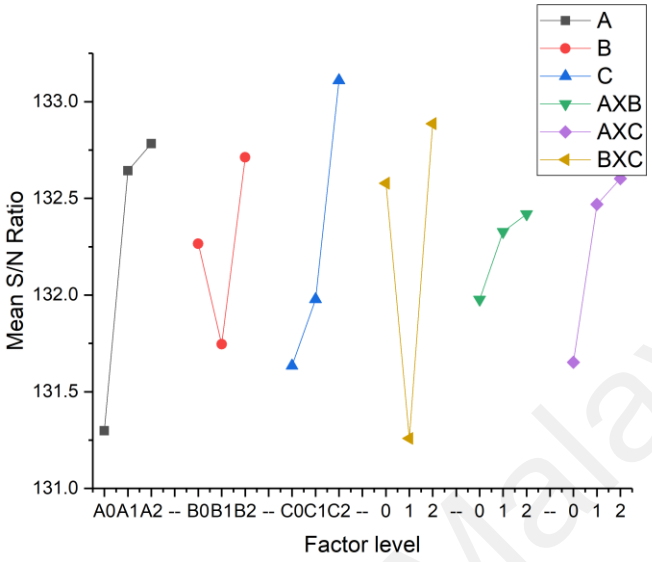

(a)

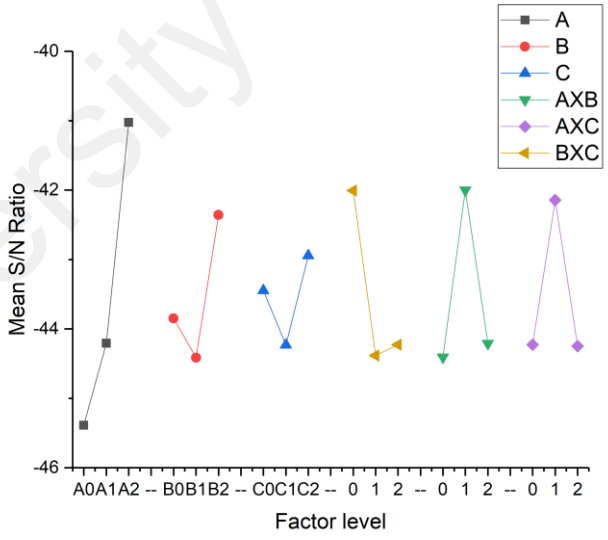

(b)

Figure 4.8 Mean S/N ratio for ±5% variation at X-Axis (a) maximum stress, (b) displacement sensitivity

Based on the Figure 4.8, the largest maximum-minimum difference obtained for interaction of maximum stress was BxC (1.627 of difference) and Table 4.4 shows the

BxC two-way table for further analysis. Meanwhile, for displacement sensitivity, the largest maximum-minimum difference obtained was AxB (2.408 of difference) and Table 4.5 shows the AxB two-way table for further analysis.

Table 4.4 BxC two-way table for maximum stress at ±5% variation on X-Axis

	B_0	B_1	B_2	Total
C_0	394.30	394.83	395.58	1184.71
C_1	392.54	397.67	397.60	1187.81
C_2	403.55	393.21	401.24	1197.99
Total	1190.39	1185.71	1194.41	

Table 4.5 AxB two-way table for displacement sensitivity at ±5% variation on X-Axis

	A_0	A_1	A_2	Total
B_0	-135.10	-131.49	-128.04	-394.62
B_1	-136.20	-132.67	-130.86	-399.73
B_2	-137.18	-133.71	-110.31	-381.21
Total	-408.48	-397.87	-369.21	

From table 4.4, the optimal result was B_2C_2 and from Figure 4.8(a), the optimal value of A was A_2. Therefore, the optimal parameters combination for maximum stress of X-axis with ±5% variation value of parameter was $A_2B_2C_2$ and from Appendix A, the optimal maximum stress was 4.83402×10^6 Pa.

From table 4.5, the optimal result was A_1B_0 and from Figure 4.8(b), the optimal value of C was C_2. Therefore, the optimal parameters combination for displacement sensitivity of X-axis with ±5% variation value of parameter was $A_1B_0C_2$ and from Appendix A, the optimal displacement sensitivity was 0.005899 μm/g.

4.3.2.2 Optimization with Variation of ±10% for X-axis

Figure 4.9 shows the graph of Mean S/N ratio at ±10% variation of parameters value.

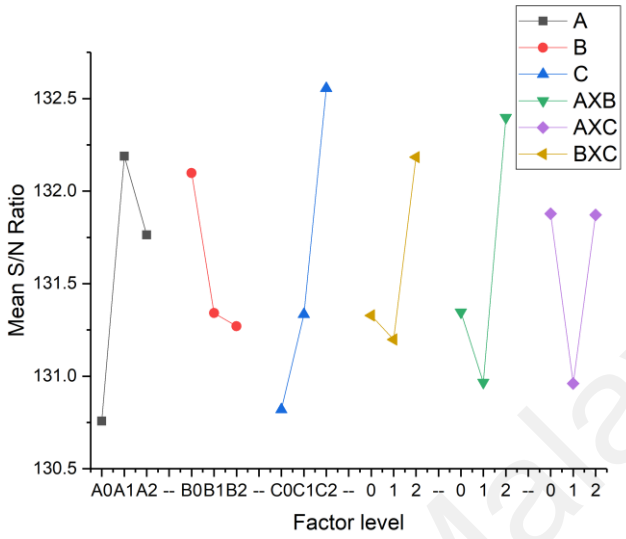

(a)

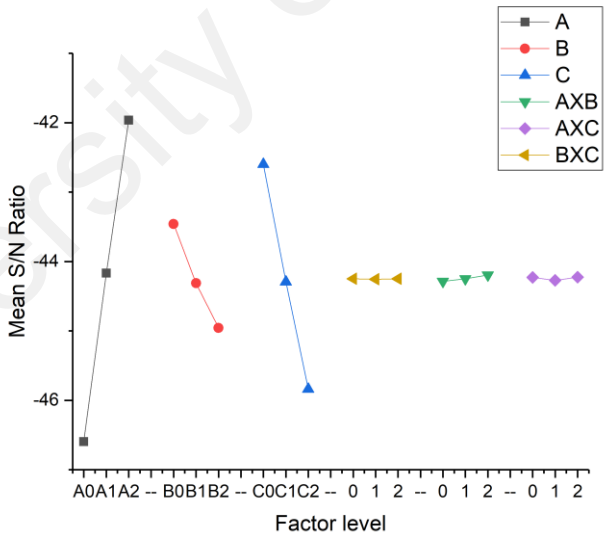

(b)

Figure 4.9 Mean S/N ratio for ±10% variation at X-Axis (a) maximum stress, (b) displacement sensitivity

Based on the Figure 4.9, the largest maximum-minimum difference obtained for interaction of maximum stress was AxB (1.432 of difference) and Table 4.6 shows the

AxB two-way table for further analysis. Meanwhile, for displacement sensitivity, the largest maximum-minimum difference obtained was AxB (0.0931 of difference) and Table 4.7 shows the AxB two-way table for further analysis.

Table 4.6 AxB two-way table for maximum stress at ±10% variation on X-Axis

	A_0	A_1	A_2	Total
B_0	394.83	396.18	397.87	1188.88
B_1	388.28	400.01	393.78	1182.07
B_2	393.70	393.51	394.23	1181.43
Total	1176.82	1189.69	1185.88	

Table 4.7 AxB two-way table for displacement sensitivity at ±10% variation on X-Axis

	A_0	A_1	A_2	Total
B_0	-137.47	-130.24	-123.42	-391.13
B_1	-140.04	-132.47	-126.29	-398.81
B_2	-141.85	-134.81	-127.95	-404.60
Total	-419.36	-397.52	-377.66	

From table 4.6, the optimal result was A_1B_0 and from Figure 4.9(a), the optimal value of C was C_2. Therefore, the optimal parameters combination for maximum stress of X-axis with ±10% variation value of parameter was $A_1B_0C_2$ and from Appendix A, the optimal maximum stress was 4.45807 x 10^6 Pa.

From table 4.7, the optimal result was A_2B_0 and from Figure 4.9(b), the optimal value of C was C_2. Therefore, the optimal parameters combination for displacement sensitivity of X-axis with ±10% variation value of parameter was $A_2B_0C_2$ and from Appendix A, the optimal displacement sensitivity was 0.007299 μm/g.

4.3.2.3 Optimization with Variation of ±15% for X-axis

Figure 4.10 shows the graph of Mean S/N ratio at ±15% variation of parameters value.

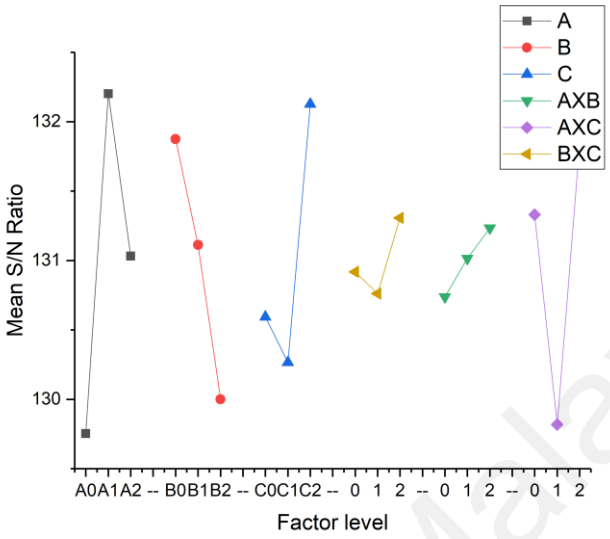

(a)

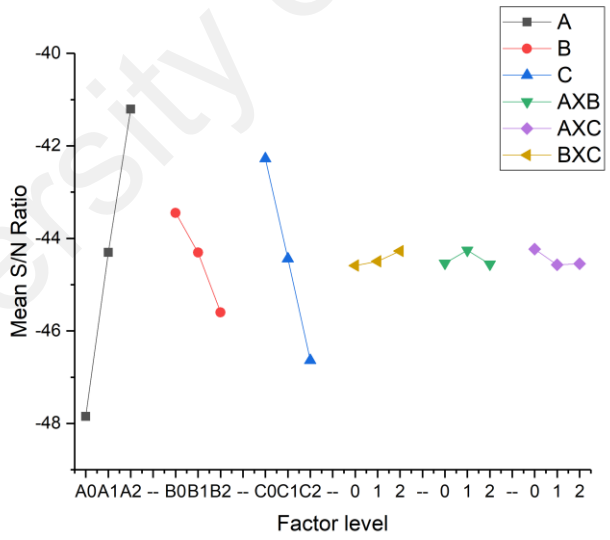

(b)

Figure 4.10 Mean S/N ratio for ±15% variation at X-Axis (a) maximum stress, (b) displacement sensitivity

Based on the Figure 4.10, the largest maximum-minimum difference obtained for interaction of maximum stress was AxC (2.019 of difference) and Table 4.8 shows the AxC two-way table for further analysis. Meanwhile, for displacement sensitivity, the largest maximum-minimum difference obtained was AxC (0.338 of difference) and Table 4.9 shows the AxC two-way table for further analysis.

Table 4.8 AxC two-way table for maximum stress at ±15% variation on X-Axis

	A_0	A_1	A_2	Total
C_0	385.51	393.88	395.95	1175.35
C_1	385.08	393.39	393.92	1172.39
C_2	397.19	402.55	389.40	1189.14
Total	1167.79	1189.81	1179.28	

Table 4.9 AxC two-way table for displacement sensitivity at ±15% variation on X-Axis

	A_0	A_1	A_2	Total
C_0	-135.93	-126.74	-117.81	-380.48
C_1	-144.29	-132.73	-122.95	-399.97
C_2	-150.40	-139.23	-130.11	-419.74
Total	-430.62	-398.71	-370.86	

From table 4.8, the optimal result was A_1C_2 and from Figure 4.10(a), the optimal value of B was B_0. Therefore, the optimal parameters combination for maximum stress of X-axis with ±15% variation value of parameter was $A_1B_0C_2$ and from Appendix A, the optimal maximum stress was 5.6939×10^6 Pa.

From table 4.9, the optimal result was A_2C_0 and from Figure 4.10(b), the optimal value of B was B_0. Therefore, the optimal parameters combination for displacement sensitivity of X-axis with ±15% variation value of parameter was $A_2B_0C_0$ and from Appendix A, the optimal displacement sensitivity was 0.009824 µm/g.

4.3.2.4 Optimization with Variation of ±20% for X-axis

Figure 4.11 shows the graph of Mean S/N ratio at ±20% variation of parameters value.

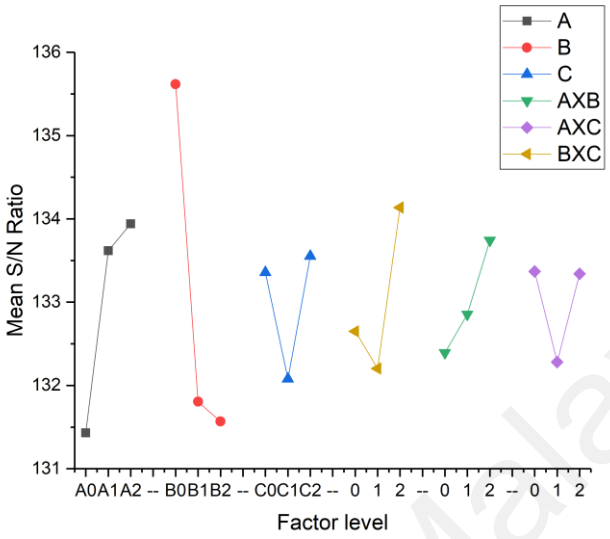

(a)

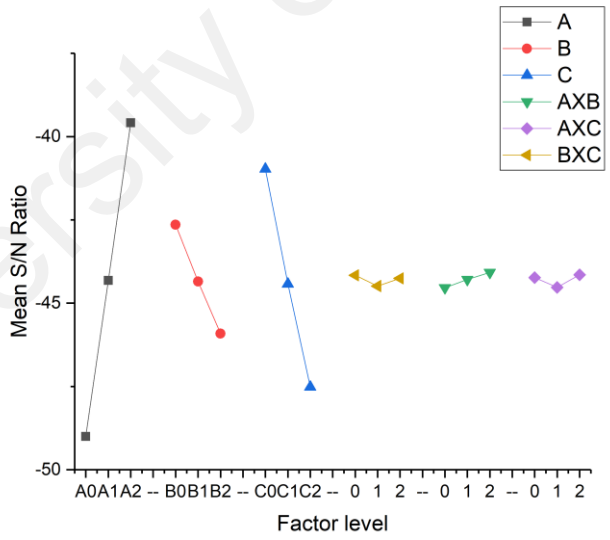

(b)

Figure 4.11 Mean S/N ratio for ±20% variation at X-Axis (a) maximum stress, (b) displacement sensitivity

Based on the Figure 4.11, the largest maximum-minimum difference obtained for interaction of maximum stress was BxC (1.932 of difference) and Table 4.10 shows the BxC two-way table for further analysis. Meanwhile, for displacement sensitivity, the largest maximum-minimum difference obtained was AxB (0.46 of difference) and Table 4.10 shows the AxB two-way table for further analysis.

Table 4.10 BxC two-way table for maximum stress at ±20% variation on X-Axis

	B_0	B_1	B_2	Total
C_0	407.05	400.19	393.59	1200.83
C_1	401.99	391.80	394.91	1188.70
C_2	412.13	394.25	395.60	1201.98
Total	1221.17	1186.24	1184.11	

Table 4.11 AxB two-way table for displacement sensitivity at ±20% variation on X-Axis

	A_0	A_1	A_2	Total
B_0	-142.34	-127.79	-113.67	-383.81
B_1	-147.66	-132.03	-119.44	-399.13
B_2	-150.99	-139.05	-123.17	-413.22
Total	-440.99	-398.88	-356.28	

From table 4.10, the optimal result was B_1C_2 and from Figure 4.11(a), the optimal value of A was A_2. Therefore, the optimal parameters combination for maximum stress of X-axis with ±20% variation value of parameter was $A_2B_1C_2$ and from Appendix A, the optimal maximum stress was 2.53641 x 10^6 Pa.

From table 4.11, the optimal result was A_2B_0 and from Figure 4.11(b), the optimal value of C was C_2. Therefore, the optimal parameters combination for displacement sensitivity of X-axis with ±20% variation value of parameter was $A_2B_0C_2$ and from Appendix A, the optimal displacement sensitivity was 0.008819 µm/g.

4.3.2.5 Optimization with Variation of ±25% for X-axis

Figure 4.12 shows the graph of Mean S/N ratio at ±25% variation of parameters value.

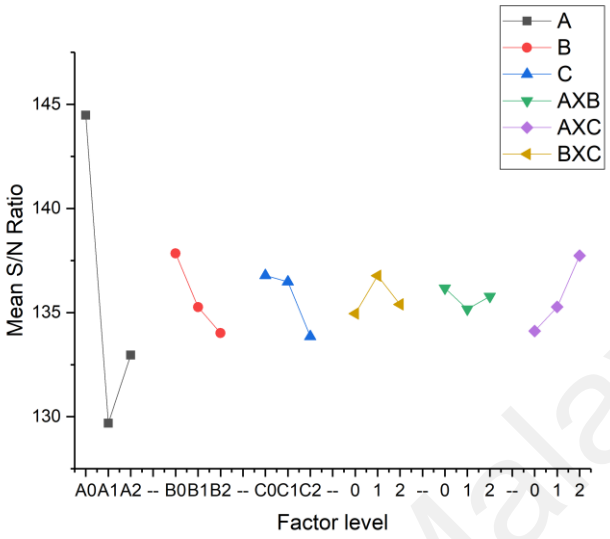

(a)

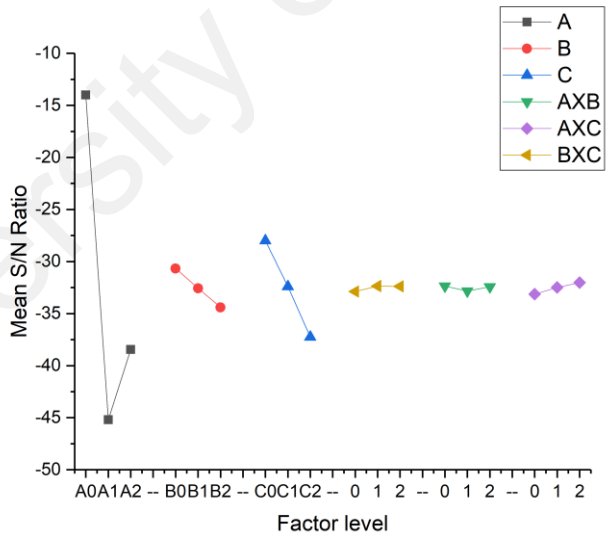

(b)

Figure 4.12 Mean S/N ratio for ±25% variation at X-Axis (a) maximum stress, (b) displacement sensitivity

Based on the Figure 4.12, the largest maximum-minimum difference obtained for interaction of maximum stress was AxC (3.617 of difference) and Table 4.12 shows the AxC two-way table for further analysis. Meanwhile, for displacement sensitivity, the largest maximum-minimum difference obtained was AxC (1.09 of difference) and Table 4.13 shows the AxC two-way table for further analysis.

Table 4.12 AxC two-way table for maximum stress at ±25% variation on X-Axis

	A_0	A_1	A_2	Total
C_0	435.21	391.58	404.31	1231.11
C_1	430.57	400.73	397.00	1228.29
C_2	434.54	374.83	395.30	1204.67
Total	1300.31	1167.14	1196.61	

Table 4.13 AxC two-way table for displacement sensitivity at ±25% variation on X-Axis

	A_0	A_1	A_2	Total
C_0	-28.52	-121.61	-101.75	-251.87
C_1	-43.05	-132.12	-116.46	-291.64
C_2	-54.40	-153.09	-127.73	-335.22
Total	-125.97	-406.82	-345.94	

From table 4.12, the optimal result was A_0C_2 and from Figure 4.12(a), the optimal value of B was B_0. Therefore, the optimal parameters combination for maximum stress of X-axis with ±25% variation value of parameter was $A_0B_0C_2$ and from Appendix A, the optimal maximum stress was 2.03653 x 10^7 Pa.

From table 4.13, the optimal result was A_0C_0 and from Figure 4.12(b), the optimal value of B was B_0. Therefore, the optimal parameters combination for displacement sensitivity of X-axis with ±25% variation value of parameter was $A_0B_0C_0$ and from Appendix A, the optimal displacement sensitivity was 0.435445 µm/g.

4.3.2.6 Optimization for X-axis of MEMS Accelerometer Summary

Based on the results obtained from 4.2.2.1 to 4.2.2.5, Table 4.14 shows the summarw of all results compared to the (Ce Zheng, 2015) results on maximum stress of X-axis and Figure 4.13 shows the graph of maximum stress on all parameters variant.

Table 4.14 Summary of maximum stress results for ±5%, ±10%, ±15%, ±20% and ±25% variation of parameters varies of X-Axis

Variant	Optimal Combination	Optimal Value	Difference with (Ce Zheng, 2015)
(Ce Zheng, 2015) Value	N/A	4.49611 x 10^6 Pa	N/A
±5%	$A_2B_2C_2$	4.83402 x 10^6 Pa	+ 7.5156%
±10%	$A_1B_0C_2$	4.45807 x 10^6 Pa	- 0.84606%
±15%	$A_1B_0C_2$	5.69396 x 10^6 Pa	+ 26.6419%
±20%	$A_2B_1C_2$	2.53641 x 10^6 Pa	- 43.5866%
±25%	$A_0B_0C_2$	20.3653 x 10^6 Pa	+ 352.954%

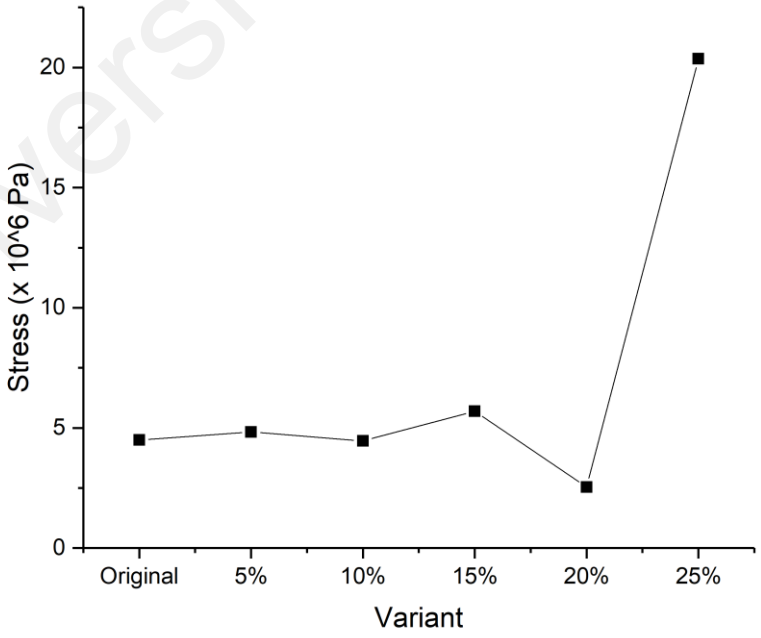

Figure 4.13 Maximum stress result of X-Axis for all five parameters variant

For displacement sensitivity, table 4.15 shows the summary of all results compared to the (Ce Zheng, 2015) results on displacement sensitivity of X-axis and Figure 4.14 shows the graph of displacement sensitivity on all parameters variant.

Table 4.15 Summary of displacement sensitivity results for ±5%, ±10%, ±15%, ±20% and ±25% variation of parameters varies of X-Axis

Variant	Optimal Combination	Optimal Value	Difference with (Ce Zheng, 2015)
(Ce Zheng, 2015) Value	N/A	0.00614 µm/g	N/A
±5%	$A_1B_0C_2$	0.005899 µm/g	- 3.9251%
±10%	$A_2B_0C_2$	0.007299 µm/g	+ 18.876%
±15%	$A_2B_0C_0$	0.009824 µm/g	+ 60%
±20%	$A_2B_0C_2$	0.008819 µm/g	+ 43.632%
±25%	$A_0B_0C_0$	0.435445 µm/g	+ 352.954%

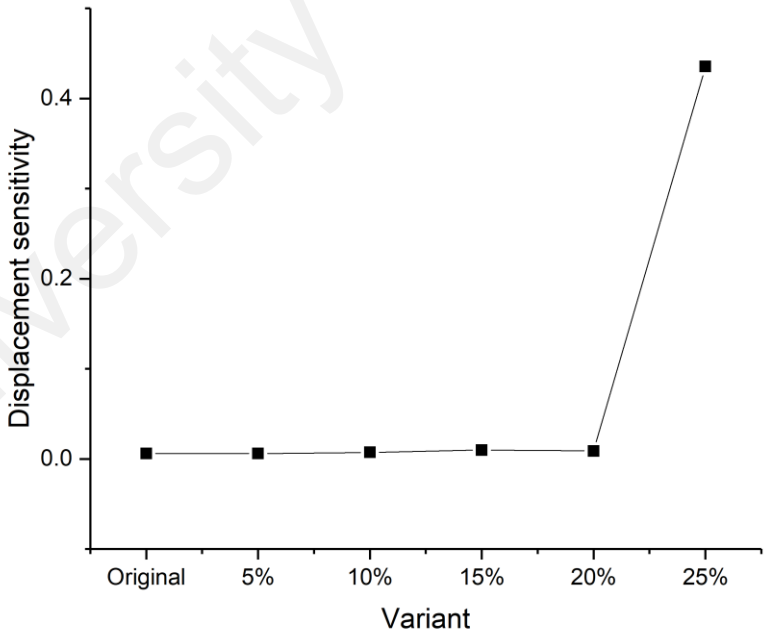

Figure 4.14 Displacement sensitivity result of X-Axis for all five parameters variant

4.4 Optimization for Y-axis of MEMS Accelerometer

4.4.1 Parameter of Y-axis Analysis

As discussed in section 3.6, five different values for three parameters which is length and width of beams and thickness of device will be done for optimization and analysis on maximum stress and displacement sensitivity of device. These three parameters have been identified as the most affected parameters for maximum stress and displacement sensitivity of this kind of device as research done by (Ce Zheng, 2015; Kaya et al., 2011; Yusof et al., 2017). The parameter values for these experiments were shown in Table 4.3 below.

Table 4.16 Parameters variant for Y- axis for each variation

Difference	Factor	Level 0, Least	Level 1, Intermediate	Level 2, Largest
± 5%	Length	1330 µm	1400 µm	1470 µm
	Width	19 µm	20 µm	21 µm
	Thickness	3.8 µm	4 µm	4.2 µm
± 10%	Length	1260 µm	1400 µm	1540 µm
	Width	18 µm	20 µm	22 µm
	Thickness	3.6 µm	4 µm	4.4 µm
± 15%	Length	1190 µm	1400 µm	1610 µm
	Width	17 µm	20 µm	23 µm
	Thickness	3.4 µm	4 µm	4.8 µm
± 20%	Length	1120 µm	1400 µm	1680 µm
	Width	16 µm	20 µm	24 µm
	Thickness	3.2 µm	4 µm	4.8 µm

± 25%	Length	1050 µm	1400 µm	1750 µm
	Width	15 µm	20 µm	25 µm
	Thickness	3 µm	4 µm	5 µm

4.4.2 Optimization Results in Y-axis

For each variation of parameters will be simulate by using COMSOL Multiphysics and Taguchi method will be applied for optimization for Y-axis. This topic will only show the graph and important results for the experiments. All detailed data were shown in Appendix B of this report.

4.4.2.1 Optimization with Variation of ±5% for Y-axis

Figure 4.15 shows the graph of Mean S/N ratio at ±5% variation of parameters value.

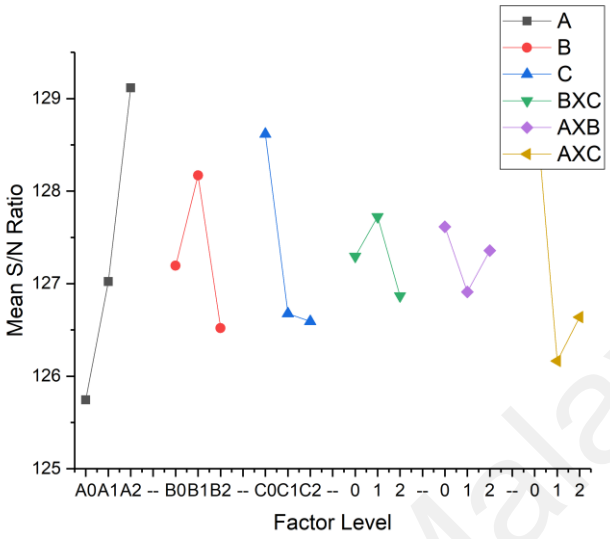

(a)

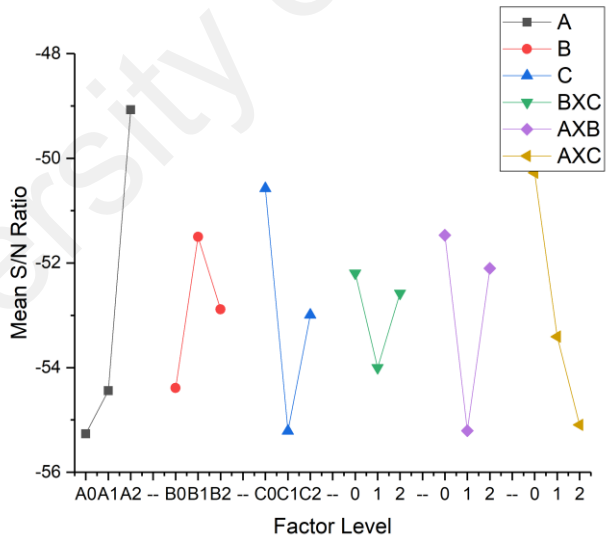

(b)

Figure 4.15 Mean S/N ratio for ±5% variation at Y-Axis (a) maximum stress, (b) displacement sensitivity

Based on the Figure 4.15, the largest maximum-minimum difference obtained for interaction of maximum stress was AxC (2.917 of difference) and Table 4.17 shows

the AxC two-way table for further analysis. Meanwhile, for displacement sensitivity, the largest maximum-minimum difference obtained was AxC (4.818 of difference) and Table 4.18 shows the AxC two-way table for further analysis.

Table 4.17 AxC two-way table for maximum stress at ±5% variation on Y-Axis

	A_0	A_1	A_2	Total
C_0	390.94	379.58	387.03	1157.55
C_1	369.67	381.63	388.79	1140.10
C_2	371.09	382.00	386.23	1139.32
Total	1131.70	1143.21	1162.05	

Table 4.18 AxC two-way table for displacement sensitivity at ±5% variation on Y-Axis

	A_0	A_1	A_2	Total
C_0	-149.19	-158.76	-147.22	-455.17
C_1	-174.65	-175.08	-147.15	-496.89
C_2	-173.55	-156.14	-147.26	-476.95
Total	-497.39	-489.98	-441.63	

From table 4.17, the optimal result was A_2C_0 and from Figure 4.15(a), the optimal value of B was B_1. Therefore, the optimal parameters combination for maximum stress of Y-axis with ±5% variation value of parameter was $A_2B_1C_0$ and from Appendix B, the optimal maximum stress was 2.7385 x 10^6 Pa.

From table 4.18, the optimal result was A_2C_0 and from Figure 4.15(b), the optimal value of B was B_1. Therefore, the optimal parameters combination for displacement sensitivity of Y-axis with ±5% variation value of parameter was $A_2B_1C_0$ and from Appendix B, the optimal displacement sensitivity was 0.003176 µm/g.

4.4.2.2 Optimization with Variation of ±10% for Y-axis

Figure 4.16 shows the graph of Mean S/N ratio at ±10% variation of parameters value.

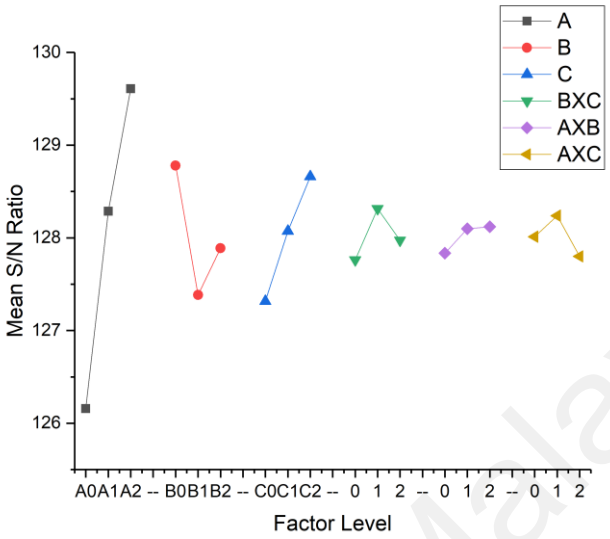

(a)

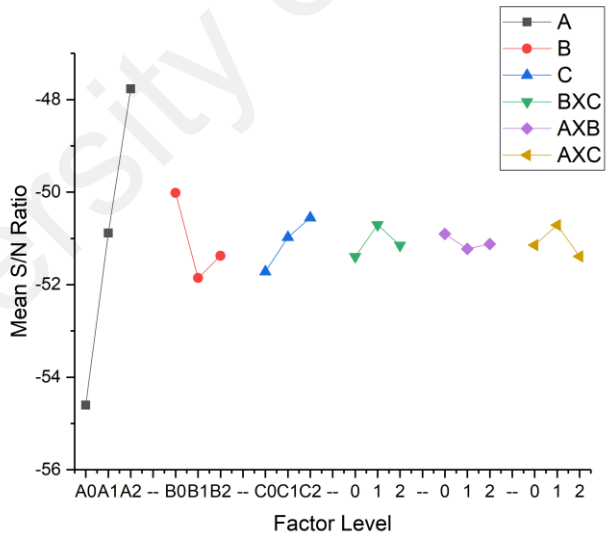

(b)

Figure 4.16 Mean S/N ratio for ±10% variation at Y-Axis (a) maximum stress, (b) displacement sensitivity

Based on the Figure 4.16, the largest maximum-minimum difference obtained for interaction of maximum stress was BxC (0.552 of difference) and Table 4.19 shows the BxC two-way table for further analysis. Meanwhile, for displacement sensitivity, the largest maximum-minimum difference obtained was BxC (0.689 of difference) and Table 4.20 shows the BxC two-way table for further analysis.

Table 4.19 BxC two-way table for maximum stress at ±10% variation on Y-Axis

	B_0	B_1	B_2	Total
C_0	383.69	378.95	383.22	1145.86
C_1	386.43	382.30	383.92	1152.65
C_2	388.90	385.19	383.86	1157.96
Total	1159.02	1146.44	1151.00	

Table 4.20 BxC two-way table for displacement sensitivity at ±10% variation on Y-Axis

	B_0	B_1	B_2	Total
C_0	-153.12	-158.19	-154.17	-465.47
C_1	-149.13	-155.45	-154.23	-458.81
C_2	-147.92	-153.06	-153.98	-454.97
Total	-450.17	-466.70	-462.39	

From table 4.19, the optimal result was B_0C_2 and from Figure 4.16(a), the optimal value of A was A_2. Therefore, the optimal parameters combination for maximum stress of Y-axis with ±10% variation value of parameter was $A_2B_0C_2$ and from Appendix B, the optimal maximum stress was 3.33921 x 10^6 Pa.

From table 4.20, the optimal result was B_0C_2 and from Figure 4.16(b), the optimal value of A was A_2. Therefore, the optimal parameters combination for displacement sensitivity of Y-axis with ±10% variation value of parameter was $A_2B_0C_2$ and from Appendix B, the optimal displacement sensitivity was 0.004630 µm/g.

4.4.2.3 Optimization with Variation of ±15% for Y-axis

Figure 4.17 shows the graph of Mean S/N ratio at ±15% variation of parameters value.

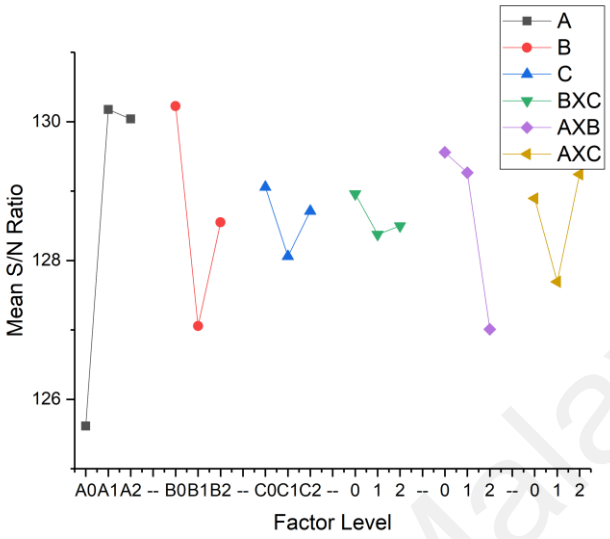

(a)

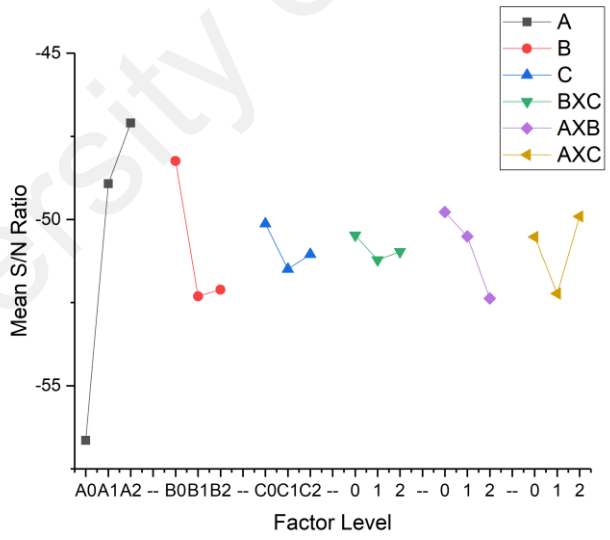

(b)

Figure 4.17 Mean S/N ratio for ±15% variation at Y-Axis (a) maximum stress, (b) displacement sensitivity

Based on the Figure 4.17, the largest maximum-minimum difference obtained for interaction of maximum stress was AxB (2.549 of difference) and Table 4.21 shows the AxB two-way table for further analysis. Meanwhile, for displacement sensitivity, the largest maximum-minimum difference obtained was AxB (2.598 of difference) and Table 4.22 shows the AxB two-way table for further analysis.

Table 4.21 AxB two-way table for maximum stress at ±15% variation on Y-Axis

	A_0	A_1	A_2	Total
B_0	387.86	393.87	390.30	1172.03
B_1	374.29	384.38	384.83	1143.50
B_2	368.40	393.33	395.22	1156.96
Total	1130.55	1171.59	1170.36	

. Table 4.22 AxB two-way table for displacement sensitivity at ±15% variation on Y-Axis

	A_0	A_1	A_2	Total
B_0	-156.08	-140.08	-138.02	-434.18
B_1	-173.23	-152.92	-144.62	-470.77
B_2	-180.44	-147.30	-141.26	-469.00
Total	-509.75	-440.29	-423.90	

From table 4.21, the optimal result was A_1B_0 and from Figure 4.17(a), the optimal value of C was C_0. Therefore, the optimal parameters combination for maximum stress of Y-axis with ±15% variation value of parameter was $A_1B_0C_0$ and from Appendix B, the optimal maximum stress was 3.17267 x 10^6 Pa.

From table 4.22, the optimal result was A_2B_0 and from Figure 4.17(b), the optimal value of C was C_0. Therefore, the optimal parameters combination for displacement sensitivity of Y-axis with ±15% variation value of parameter was $A_2B_0C_0$ and from Appendix B, the optimal displacement sensitivity was 0.007060 μm/g.

4.4.2.4 Optimization with Variation of ±20% for Y-axis

Figure 4.18 shows the graph of Mean S/N ratio at ±20% variation of parameters value.

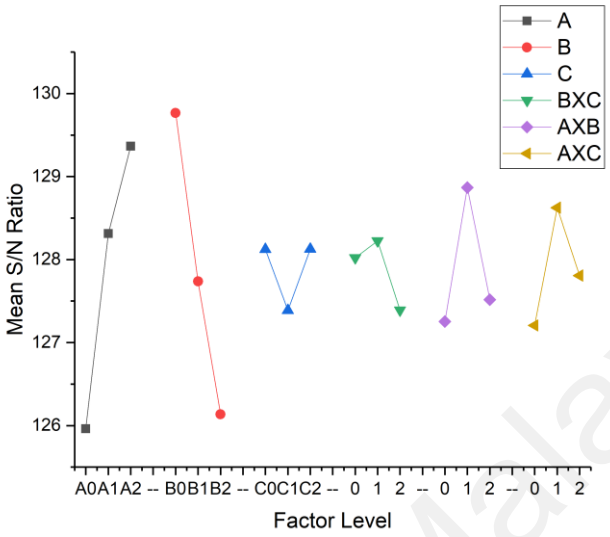

(a)

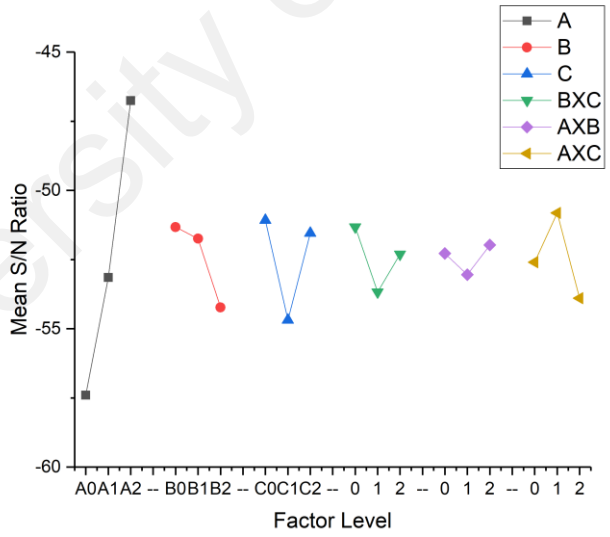

(b)

Figure 4.18 Mean S/N ratio for ±20% variation at Y-Axis (a) maximum stress, (b) displacement sensitivity

Based on the Figure 4.18, the largest maximum-minimum difference obtained for interaction of maximum stress was AxB (1.614 of difference) and Table 4.23 shows the AxB two-way table for further analysis. Meanwhile, for displacement sensitivity, the largest maximum-minimum difference obtained was AxC (3.082 of difference) and Table 4.24 shows the AxC two-way table for further analysis.

Table 4.23 AxB two-way table for maximum stress at ±20% variation on Y-Axis

	A_0	A_1	A_2	Total
B_0	382.50	393.51	391.90	1167.90
B_1	379.65	384.26	385.73	1149.63
B_2	371.50	377.05	386.66	1135.22
Total	1133.65	1154.82	1164.29	

Table 4.24 AxC two-way table for displacement sensitivity at ±20% variation on Y-Axis

	A_0	A_1	A_2	Total
C_0	-176.10	-146.83	-136.75	-459.68
C_1	-170.27	-178.07	-143.85	-492.18
C_2	-170.24	-153.39	-140.22	-463.85
Total	-516.61	-478.29	-420.82	

From table 4.23, the optimal result was A_2B_0 and from Figure 4.18(a), the optimal value of C was C_2. Therefore, the optimal parameters combination for maximum stress of Y-axis with ±20% variation value of parameter was $A_2B_0C_2$ and from Appendix B, the optimal maximum stress was 2.91385 x 10^6 Pa.

From table 4.24, the optimal result was A_2C_0 and from Figure 4.18(b), the optimal value of B was B_0. Therefore, the optimal parameters combination for displacement sensitivity of Y-axis with ±20% variation value of parameter was $A_2B_0C_0$ and from Appendix B, the optimal displacement sensitivity was 0.009443 μm/g.

4.4.2.5 Optimization with Variation of ±25% for Y-axis

Figure 4.19 shows the graph of Mean S/N ratio at ±25% variation of parameters value.

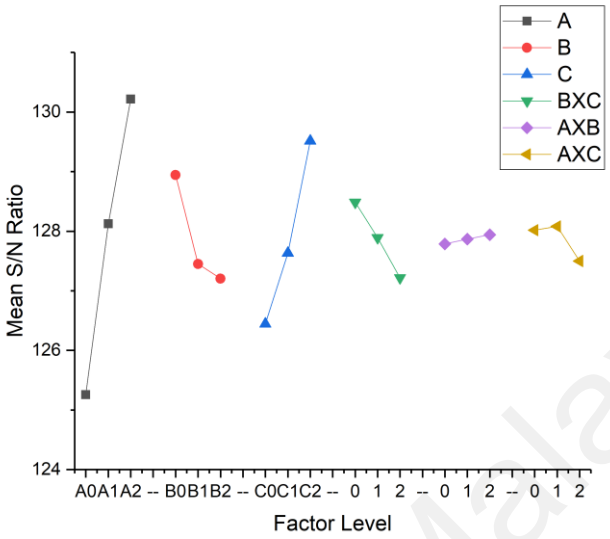

(a)

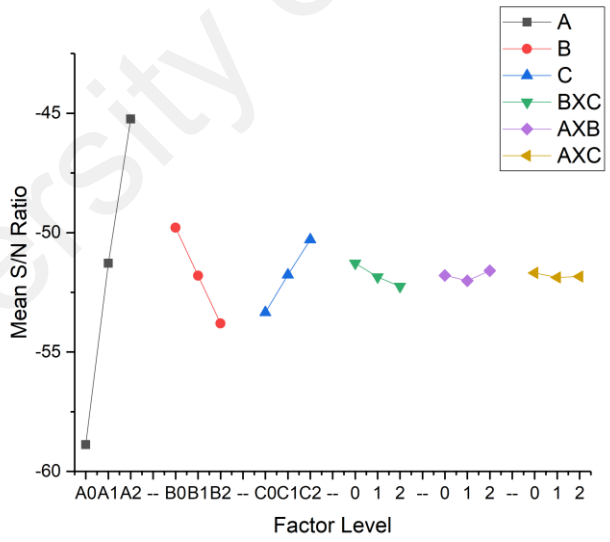

(b)

Figure 4.19 Mean S/N ratio for ±25% variation at Y-Axis (a) maximum stress, (b) displacement sensitivity

Based on the Figure 4.19, the largest maximum-minimum difference obtained for interaction of maximum stress was BxC (1.268 of difference) and Table 4.25 shows the BxC two-way table for further analysis. Meanwhile, for displacement sensitivity, the largest maximum-minimum difference obtained was BxC (0.969 of difference) and Table 4.26 shows the BxC two-way table for further analysis.

Table 4.25 BxC two-way table for maximum stress at ±25% variation on Y-Axis

	B_0	B_1	B_2	Total
C_0	384.50	375.98	377.54	1138.02
C_1	386.03	383.62	379.06	1148.71
C_2	389.93	387.45	388.25	1165.64
Total	1160.47	1147.05	1144.85	

Table 4.26 BxC two-way table for displacement sensitivity at ±25% variation on Y-Axis

	B_0	B_1	B_2	Total
C_0	-152.30	-161.50	-166.26	-480.06
C_1	-149.59	-153.81	-162.51	-465.91
C_2	-146.27	-150.90	-155.47	-452.64
Total	-448.16	-466.21	-484.24	

From table 4.25, the optimal result was B_0C_2 and from Figure 4.19(a), the optimal value of A was A_2. Therefore, the optimal parameters combination for maximum stress of Y-axis with ±25% variation value of parameter was $A_2B_0C_2$ and from Appendix B, the optimal maximum stress was 4.48025 x 10^6 Pa.

From table 4.26, the optimal result was B_0C_2 and from Figure 4.19(b), the optimal value of A was A_2. Therefore, the optimal parameters combination for displacement sensitivity of Y-axis with ±25% variation value of parameter was $A_2B_0C_2$ and from Appendix B, the optimal displacement sensitivity was 0.009370 µm/g.

4.4.2.6 Optimization for Y-axis of MEMS Accelerometer Summary

Based on the results obtained from 4.3.2.1 to 4.3.2.5, Table 4.27 shows the summary of all results compared to the (Ce Zheng, 2015) results on maximum stress of Y-axis and Figure 4.20 shows the graph of maximum stress on all parameters variant.

Table 4.27 Summary of maximum stress results for ±5%, ±10%, ±15%, ±20% and ±25% variation of parameters varies of Y-Axis

Variant	Optimal Combination	Optimal Value	Difference with (Ce Zheng, 2015)
(Ce Zheng, 2015) Result	N/A	2.53323×10^{6} Pa	N/A
±5%	$A_2B_1C_0$	2.7385×10^{6} Pa	+ 8.10309%
±10%	$A_2B_0C_2$	3.33921×10^{6} Pa	+ 31.8163%
±15%	$A_1B_0C_0$	3.17267×10^{6} Pa	+ 25.2421%
±20%	$A_2B_0C_2$	2.91385×10^{6} Pa	+ 15.0250%
±25%	$A_2B_0C_2$	4.48025×10^{6} Pa	+ 76.8592%

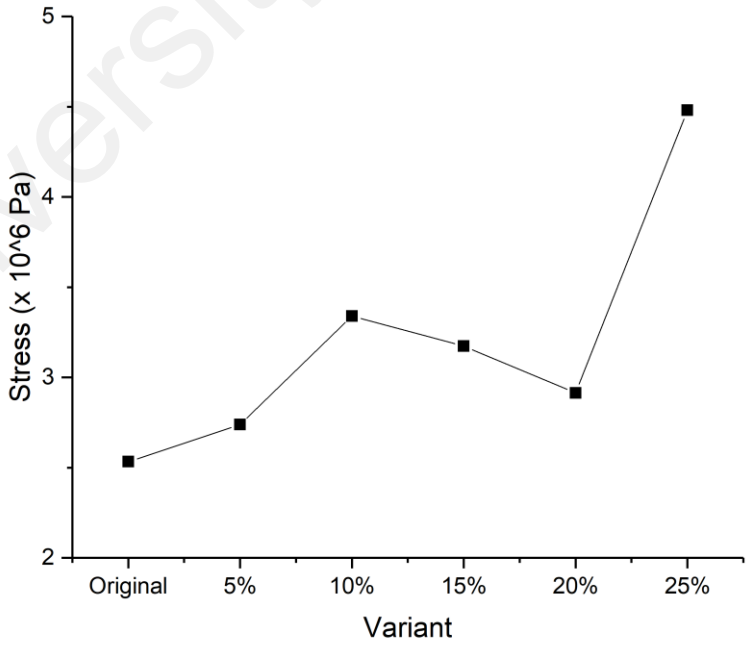

Figure 4.20 Maximum stress result of Y-Axis for all five parameters variant

For displacement sensitivity, table 4.28 shows the summary of all results compared to the (Ce Zheng, 2015) results on displacement sensitivity of Y-axis and Figure 4.21 shows the graph of displacement sensitivity on all parameters variant.

Table 4.28 Summary of displacement sensitivity results for ±5%, ±10%, ±15%, ±20% and ±25% variation of parameters varies of Y-Axis

Variant	Optimal Combination	Optimal Value	Difference with (Ce Zheng, 2015)
(Ce Zheng, 2015) Results	N/A	0.002873 µm/g	N/A
±5%	$A_2B_1C_0$	0.003176 µm/g	+ 10.5465%
±10%	$A_2B_0C_2$	0.004630 µm/g	+ 61.1556%
±15%	$A_2B_0C_0$	0.007060 µm/g	+ 145.7362%
±20%	$A_2B_0C_0$	0.009443 µm/g	+ 228.6808%
±25%	$A_2B_0C_2$	0.009370 µm/g	+ 226.1399%

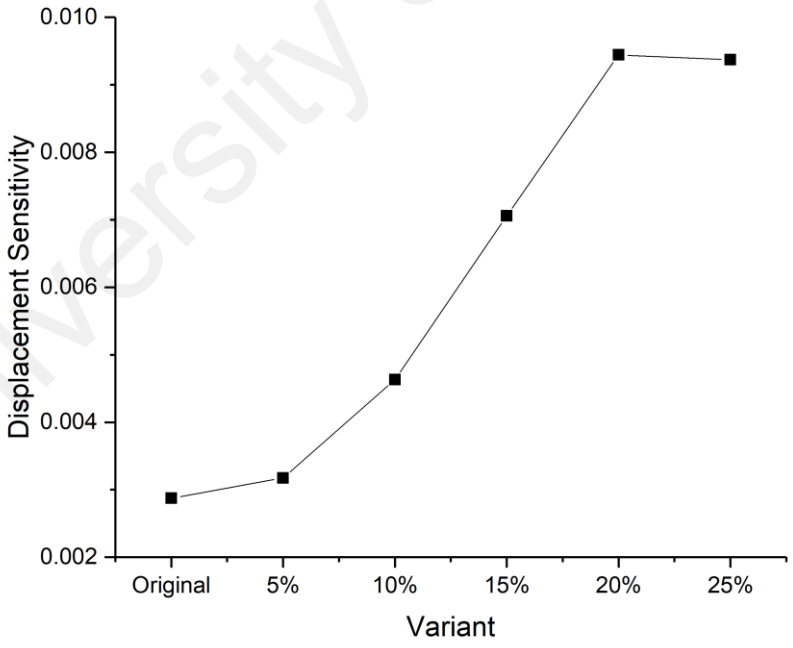

Figure 4.21 Displacement sensitivity result of Y-Axis for all five parameters variant

4.5 Taguchi Method Optimization Analysis

Maximum stress for MEMS accelerometer of this dual-axis design might be affected due to three parameters that have been shared in 4.3 and 4.4. (Ce Zheng, 2015) mention that the bending displacement of the beams will provide the different value of maximum stress and it is proportional to the inertia force $F_{inertial}$, which is also proportional to input acceleration:

$$F_{inertial} = -M_s . a \tag{4.3}$$

$$x = F_{inertial}/K_{xtot} \tag{4.4}$$

$$y = F_{inertial}/K_{ytot} \tag{4.5}$$

Where M_s is the mass of the sensing mass, and a is the input acceleration, K_{xtot} and K_{ytot} are the effective spring constants of the beams along X and Y directions.

For the displacement sensitivity, it was defined as the displacement of the beams per 1g acceleration input along the sensitive direction. The displacement sensitivities of the accelerometer along Y and X directions are:

$$S_{dx} = \frac{\rho(w_m \cdot L_m \cdot t_m + 64 \cdot w_f \cdot L_f \cdot t_f) \cdot g \cdot {L_{bx}}^3}{2E \cdot {w_{bx}}^3 \cdot t_{bx}} \tag{4.6}$$

$$S_{dy} = \frac{\rho(w_m \cdot L_m \cdot t_m + 64 \cdot w_f \cdot L_f \cdot t_f) \cdot g \cdot {L_{by}}^3}{2E \cdot {w_{by}}^3 \cdot t_{by}} \quad (4.7)$$

Based on the above analysis, it can be seen that the sensitivity can be improved by adjusting the beam width, length and thickness. Adjusting these three parameters is an effective way because it will not affecting the overall device area (Ce Zheng, 2015; Kaya et al., 2011; Yusof et al., 2017).

From the results of both Y-axis and X-axis, we can see from table 4.14 and table 4.15 for X-axis and table 4.27 and table 4.28 for Y-axis, 65% (13 out of 20) of the optimal results was obtained when the device's thickness was at maximum. This proves the theory that when the higher thickness, the higher force must be applied as equation 3.1 from chapter 3 of this report, by this, it will obtain the higher maximum stress and displacement.

For the X-axis results, it shows that with the increase of 25% variation for these three parameters, the optimum maximum stress and displacement sensitivity have maximum of improvement of 352% compared to the original results. However, although it obtained the highest maximum stress and displacement sensitivity, due to the design limitation, the result can be ignored because it apply the smallest value of length and width as Figure 4.22 which also means that the design was not practical when it was near to the moveable comb as studied by (Kaya et al., 2011).

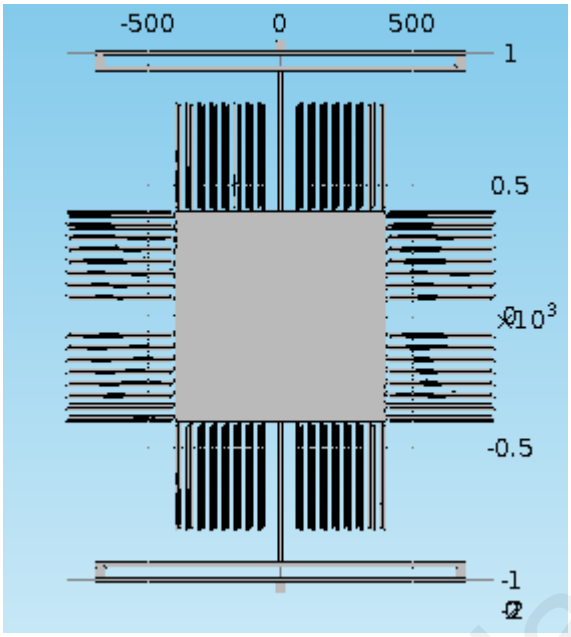

Figure 4.22 Design with minimum length and width of X-beam

For the second highest improvement, which is when 15% of improvements, both maximum stress and displacement sensitivity will be obtained with 26.6% and 60% of improvement with the length of 700µm, width of 17µm and thickness of 23µm. The design with this configuration was as Figure 4.23.

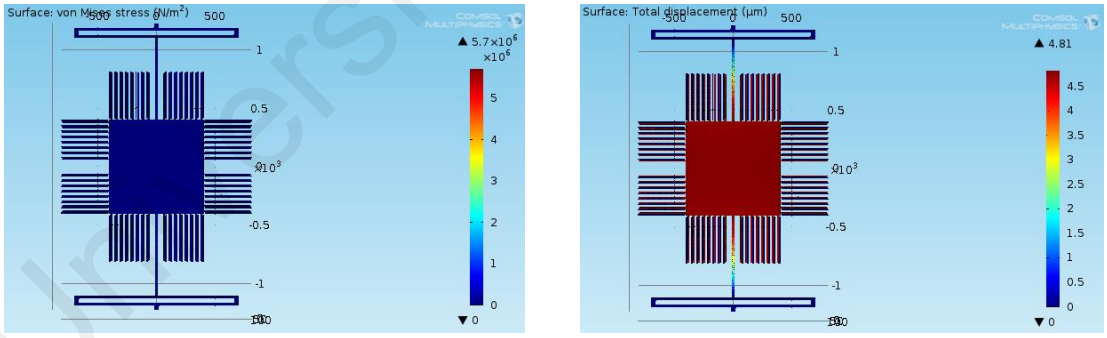

(a) (b)

Figure 4.23 Design with optimal (a) maximum stress, and (b) displacement sensitivity for X-axis

For Y-axis results, the best combination of getting the optimal both displacement sensitivity and maximum stress is when 10% of variant where maximum

stress give 31.8% of improvements while displacement sensitivity give 61.2% of improvements. Figure 4.24 show the combination that gives the optimal results.

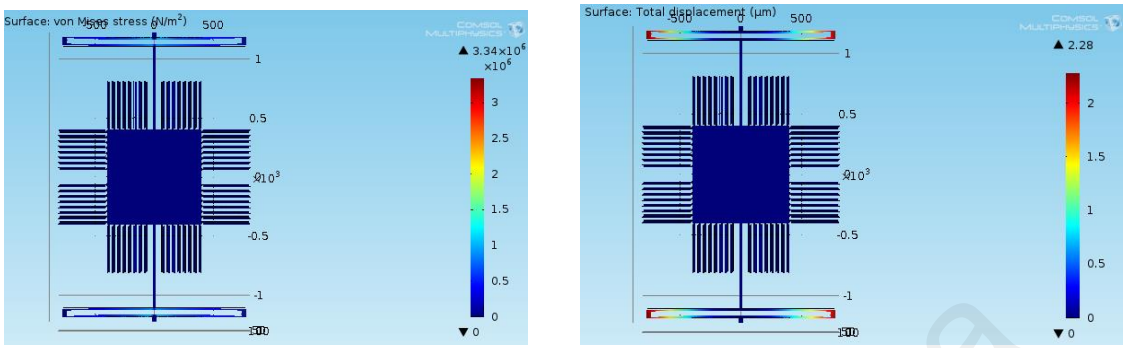

(a) (b)

Figure 4.24 Design with optimal (a) maximum stress, and (b) displacement sensitivity for Y-axis

4.5.1 Pareto ANOVA Analysis

One of the other methods to analyse data for process optimization as mention in chapter 3 is the use of Pareto ANOVA. Therefore, next step of analyzation is applied the Pareto ANOVA technique. Figure 4.25 shows the pareto diagram of contribution ratio for each factor and interaction. The interaction studied for this analysis was only AxB, AxC and BxC and AxB(11), AxC(12) and BxC(12) can be ignored as mentioned by (Ghani, Choudhury, & Hassan, 2004)

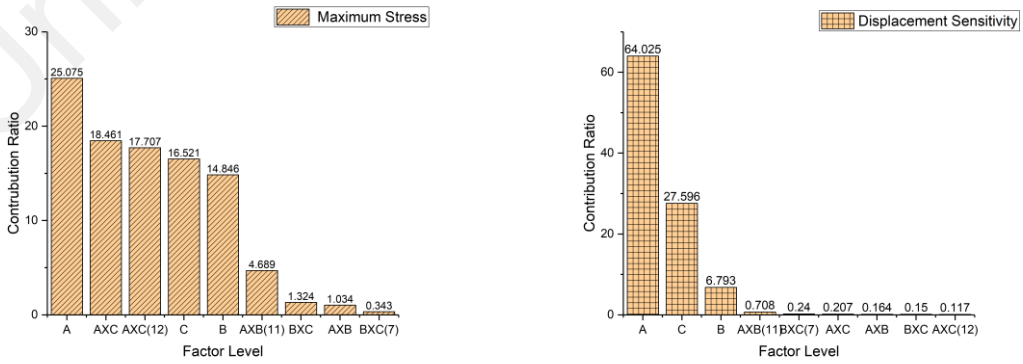

(a) (b)

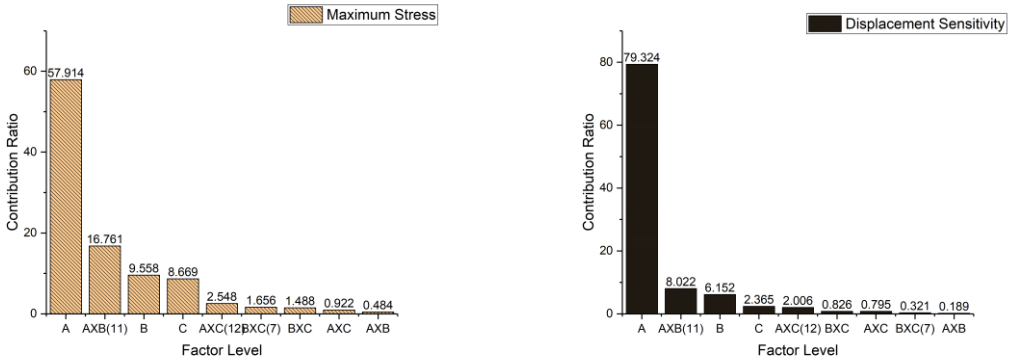

(c) (d)

Figure 4.25 Pareto diagram of contribution ratio for each factor and interaction (a) & (b) for X-axis, (c) & (d) for Y-axis

For the X-axis, as shown in Figure 4.24(a) and Figure 4.24(b), length (factor A) of the X-beam was found to be a dominant followed by thickness of device (factor C) as the single factors. While for the interaction, we can see it actually a higher dominant (rank 2) for maximum stress at the X-axis with factor A interaction with factor C as the dominant. However, for displacement sensitivity, the single factor was most dominant compared to the interaction. As length and thickness give the highest interaction (AxC), both factors were chosen to obtain the optimum maximum stress and displacement sensitivity.

Next, the Y-axis pareto ANOVA shows that length (factor A) of the Y-beam was the most dominant. The interaction between width and thickness (BxC) give the highest interaction and these factors were chosen to obtain the optimum maximum stress and displacement sensitivity.

CHAPTER 5 : CONCLUSION

5.1 Conclusion

For this research project, a capacitive MEMS accelerometer that can be applied on lower limb exoskeleton is studied. The maximum stress and displacement sensitivity of device is predicted and simulated. By using the analytical method, the COMSOL Multiphysics simulation is used to confirm the relationship between the device maximum stress and displacement sensitivity with numerous of its design parameters.

Based on the simulation, the different setup parameters on length and width of X and Y beam, as well as the thickness of the device will result the different value of maximum stress and displacement sensitivity where it all matched with the theoretical analysis. As there are three parameters modified, the Taguchi Method applied gives the optimum results for both maximum stress and displacement sensitivity for X and Y beams.

As a conclusion, for X-axis, with ±15% variation of length and width of X-beam and thickness of device parameter value was the best setup with maximum stress of **5.69396 x 10^6 Pa** and displacement sensitivity of **0.009824 µm/g** which gives **26.6419%** and **60%** of improvements. Meanwhile, for Y-axis, ±10% variation of length and width of Y-beam and thickness of device of parameters value was the best setup with maximum stress of **3.33921 x 10^6 Pa** and displacement sensitivity of **0.004630 µm/g** which gives **31.8163%** and **61.1556%** of improvements.

5.2 Recommendation for Future Work

This research is a simulation-based project. In future, it is good to develop the real device by using suggested parameters to obtain the maximum stress and displacement sensitivity. Later, this developed device will be assigned in the lower limb

exoskeleton to run another of experiments on sensitivity because as discussed in introduction, this is limitation of projects where it is not able to run and applied with the exoskeleton.

REFERENCES

Andrejašic, M. (2008). *Mems accelerometers.* Paper presented at the University of Ljubljana. Faculty for mathematics and physics, Department of physics, Seminar.

Beeby, S. (2004). *MEMS mechanical sensors*: Artech House.

Benichou, A., Benmoussa, N., & Ghaffour, K. (2013). STUDY OF A THREE-AXIS PIEZORESISTIVE ACCELEROMETER WITH UNIFORM AXIAL SENSITIVITIES. *European Scientific Journal, ESJ, 9*(21).

Ce Zheng, X. X., Junling Hu. (2015). *COMSOL Simulation of a Dual-axis MEMS Accelerometer with T-shape Beams*. Paper presented at the Conference: 2015 COMSOL Boston Conference.

Chunhui, D., Changde, H., Jiaqi, Y., Xiaoyang, G., Yongping, Z., & Wendong, Z. (2012). Design and measurement of a piezoresistive triaxial accelerometer based on MEMS technology. *Journal of Semiconductors, 33*(10), 104005.

Denishev, K. H., & Petrova, M. R. (2007). Accelerometer design. *Proceedings of ELECTRONICS, 2007*, 159-164.

Ghani, J. A., Choudhury, I., & Hassan, H. (2004). Application of Taguchi method in the optimization of end milling parameters. *Journal of materials processing technology, 145*(1), 84-92.

Gogoi, B. P., & Mladenovic, D. (2002). *Integration technology for MEMS automotive sensors.* Paper presented at the IECON 02 [Industrial Electronics Society, IEEE 2002 28th Annual Conference of the].

Huang, R., Cheng, H., Guo, H., Lin, X., Chen, Q., & Sun, F. (2016). *Learning Cooperative Primitives with physical Human-Robot Interaction for a HUman-powered Lower EXoskeleton.* Paper presented at the Intelligent Robots and Systems (IROS), 2016 IEEE/RSJ International Conference on.

Kaya, T., Shiari, B., Petsch, K., & Yates, D. (2011). Design of a MEMS Capacitive Comb-drive Accelerometer. *Central Michigan University, University of Michigan*.

Khairun Nisa, K. (2014). *Design And Analysis Of MEMS Capacitive Accelerometer With Optimized Sensitivity.* Universiti Teknikal Malaysia Melaka.

Lee, I., Yoon, G. H., Park, J., Seok, S., Chun, K., & Lee, K.-I. (2005). Development and analysis of the vertical capacitive accelerometer. *Sensors and Actuators A: Physical, 119*(1), 8-18.

Luo, Y. (2013). *Cross-axis sensitivity enhancement for a quad beam piezoresistive accelerometer.* Paper presented at the Electrical and Computer Engineering (CCECE), 2013 26th Annual IEEE Canadian Conference on.

Lyshevski, S. E. (2002). *MEMS and NEMS: systems, devices, and structures*: CRC press.

Messina, M., & Njuguna, J. (2012). *Potential of silicon nanowires structures as nanoscale piezoresistors in mechanical sensors.* Paper presented at the IOP Conference Series: Materials Science and Engineering.

Moreno, J., Freriks, B., Porsteinsson, F., Sánchez, J., & Pons, J. (2004). *Intelligent knee-ankle-foot orthosis: The gait project approach.* Paper presented at the INTERNATIONAL JOURNAL OF REHABILITATION RESEARCH.

Multiphysics, C. (2013). Structural Mechanics Module User's Guide. In COMSOL (Ed.).

Olivares, A., Olivares, G., Gorriz, J., & Ramirez, J. (2009). *High-efficiency low-cost accelerometer-aided gyroscope calibration.* Paper presented at the Test and Measurement, 2009. ICTM'09. International Conference on.

Rocon, E., Moreno, J., Ruiz, A., Brunetti, F., Miranda, J., & Pons, J. (2007). *Application of inertial sensors in rehabilitation robotics.* Paper presented at the 2007 IEEE 10th International Conference on Rehabilitation Robotics.

Sabatini, A. M. (2011). Estimating three-dimensional orientation of human body parts by inertial/magnetic sensing. *Sensors, 11*(2), 1489-1525.

Sankar, A. R., Das, S., & Lahiri, S. (2009). Cross-axis sensitivity reduction of a silicon MEMS piezoresistive accelerometer. *Microsystem Technologies, 15*(4), 511-518.

Shah, M. A., Iqbal, F., & Lee, B.-L. (2016). *Design and analysis of a single-structure three-axis MEMS gyroscope with improved coupling spring.* Paper presented at the Nano/Micro Engineered and Molecular Systems (NEMS), 2016 IEEE 11th Annual International Conference on.

Shah, M. A., Iqbal, F., Shah, I. A., & Lee, B. (2016). Modal Analysis of a Single-Structure Multiaxis MEMS Gyroscope. *Journal of Sensors, 2016*.

Sharma, K., Macwan, I., Zhang, L., Hmurcik, L. V., & Xiong, X. (2007). *Design optimization of MEMS comb accelerometer*.

Souza, F. (2015). Arduino - Interface with accelerometer and gyroscope. from https://www.embarcados.com.br/arduino-acelerometro-giroscopio/

Stefan Lambrecht, S. L. N., Magdo Bortole, Adriano A. G. Siqueira, Marco H. Terra, Eduardo Rocon, José L. Pons. (2016). Inertial Sensor Error Reduction through Calibration and Sensor Fusion. *Sensors 2016, 16, 235, 16*, 235.

Sung, J., Kim, J. Y., Seok, S., Kwon, H. J., Kim, M., Kim, G., & Lim, G. (2014). A gyroscope fabrication method for high sensitivity and robustness to fabrication tolerances. *Journal of Micromechanics and Microengineering, 24*(7), 075013.

Tim, S. (1996). *Accelerometer (ADXL50). Human computer interface design.*, Stanford University.

Vijila, G., Vijayakumar, S., & Gupta, A. M. A. (2011). *Design and Analysis of 3D Capacitive Accelerometer for Automotive Applications.* Paper presented at the The COMSOL Conference.

Widas, P. (1997). Introduction to Finite Element Analysis. from http://www.sv.rkriz.net/classes/MSE2094_NoteBook/97ClassProj/num/widas/history.html

Xiong, X. (2005). *Built-in self-test and self-repair for capacitive MEMS devices.* University of Cincinnati.

Yusof, N., Soinb, N., & Noorakma, A. C. (2017). Effect of Beams Structures on Dynamic Behavior of Piezoresistive Accelerometer Sensors. *Journal of Telecommunication, Electronic and Computer Engineering (JTEC), 9*(1-4), 77-81.